

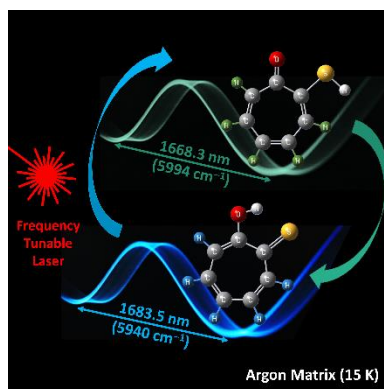
Bond-Breaking/Bond-Forming Reactions by Vibrational Excitation: Infrared-Induced Bidirectional Tautomerization of Matrix-Isolated Thiotropolone

Cláudio M. Nunes,^{1*} Nelson A. M. Pereira,¹ Igor Reva,¹ Patrícia S. M. Amado,² Maria L. S. Cristiano,² and Rui Fausto¹

¹University of Coimbra, CQC, Department of Chemistry, 3004-535 Coimbra, Portugal

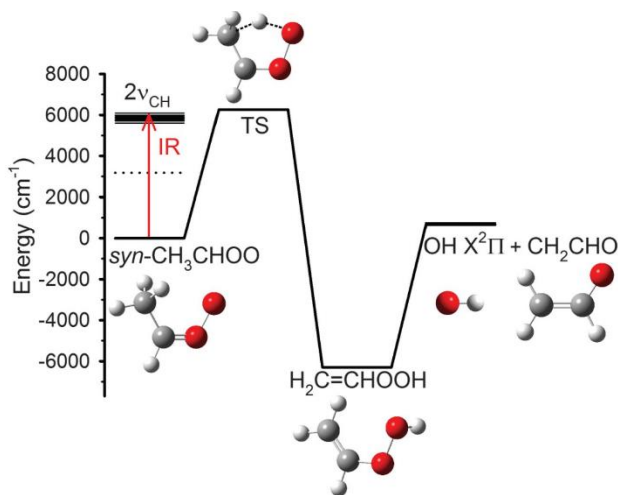
²Center of Marine Sciences, CCMAR, and Department of Chemistry and Pharmacy, University of Algarve, 8005-139 Faro, Portugal

*cmnunes@qui.uc.pt



ABSTRACT: Infrared vibrational excitation is a promising approach to get exceptional control of chemical reactions, in ways not attainable via thermal or electronic excitation. Here, we report an unprecedented example of a bond-breaking/bond-forming reaction by vibrational excitation under matrix-isolation conditions. Thiotropolone monomers were isolated in cryogenic argon matrices and characterized by infrared spectroscopy and vibrational computations (harmonic and anharmonic). Narrowband near-infrared irradiations tuned at frequencies of first CH stretching overtone (5940 cm^{-1}) or combination modes (5980 cm^{-1}) of the OH-tautomer, the sole form of the compound existing in the as-deposited matrices, led to its conversion into the SH-tautomer. The tautomerization in the reverse direction was achieved by vibrational excitation of the SH-tautomer with irradiations at 5947 or 5994 cm^{-1} , corresponding to the frequencies of its CH stretching combination and overtone modes. This pioneer demonstration of bidirectional hydroxyl \leftrightarrow thiol tautomerization controlled by vibrational excitation creates prospects for new advances in vibrationally induced chemistry.

Selective energy deposition in a chosen vibrational mode of a given molecular species is a promising way to achieve exquisite control of chemical reactions.¹⁻⁷ This approach contrasts with conventional heating, in which energy is non-selectively deposited in all molecules of the considered system. The dream of tuning light at a vibrational frequency of a particular bond and induce a chemical reaction only at that site is extremely challenging, even using femtosecond pulses at low-pressure gas-phase conditions.⁸ This is partially because intramolecular vibrational energy redistribution (IVR) dissipates the deposited energy fast to other modes before the reaction arises.^{5,9} Alternatively, if a dominant (nonstatistical) IVR pathway exists due to the coupling between an excited vibrational mode and a reaction coordinate, this might be exploited to induce a desired chemical transformation in an elegant and selective way.^{3,10} One remarkable example illustrating this possibility is the vibrationally induced unimolecular reaction of the jet-cooled Criegee intermediate *syn*-CH₃CHOO, reported by Lester et al.¹¹⁻¹⁴ The authors demonstrated that excitation of CH stretching overtones or combination modes induces a 1,4-H shift from the methyl group to the terminal oxygen and activates the molecule decomposition (Scheme 1).¹¹ Nevertheless, the application of this strategy to induce and control organic reactions still remains scarcely explored.¹⁵⁻²⁴

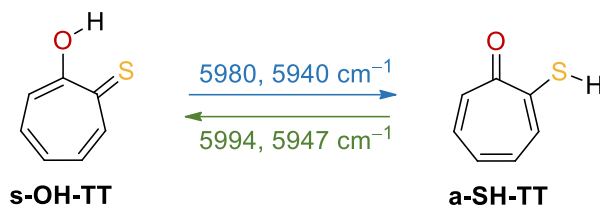


Scheme 1. Reaction of a Criegee intermediate (*syn*-CH₃CHOO) induced by pumping $2\nu(\text{CH})$ overtones with narrowband light tuned at $\sim 6000\text{ cm}^{-1}$ (note the red vertical arrow). Adapted from Ref. 11 with permission from Science.

One noticeable exception has been the use of vibrational excitation to manipulate molecular conformations of different classes of organic compounds.²⁵⁻⁴⁵ In general, such

transformations are explored with help of the low-temperature matrix isolation technique, which provides ideal conditions for investigating chemical processes with low energy barriers, suitable to be activated by IR light.²⁵ Typically, energy is deposited in XH (X = O or N) first stretching overtones, because these modes have substantial energy alongside with a significant enough absorption cross-section.⁴⁶ This way, it has been shown that vibrational excitation can induce rotamerization of a light H-atom (e.g. of an OH or SH group)^{26,27,31,33,34,37,38,40,41,45} or heavy fragments (e.g. aldehyde,²⁸ hydroxymethyl,^{32,42} methoxy³⁵), even when they are located remotely in relation to the excited vibrational mode. To the best of our knowledge, apart from conformational isomerizations, only one other type of reaction induced by vibrational excitation under matrix isolation conditions has been reported hitherto,^{47,48} namely the reaction of small ethylene derivatives aggregated with F₂.^{49–51}

Here, we demonstrate an unprecedented example of a bond-breaking/bond-forming reaction activated by vibrational excitation under matrix-isolation conditions, namely the hydroxyl ↔ thiol tautomerization of thiotropolone (**TT**), which can be induced in both directions by excitation of CH stretching overtones or combination modes of the corresponding reactant species (Scheme 2).

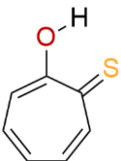
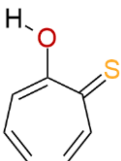
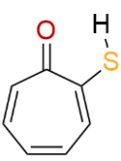
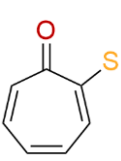


Scheme 2. Bidirectional tautomerizations in thiotropolone (**TT**) induced by vibrational excitation. In the names of structures, **s** stands for *syn* and **a** stands for *anti*, corresponding to the orientation of the O–H/S=C or S–H/O=C moieties.

Thiotropolone was prepared by standard procedures, as described in the Supporting Information (SI). The compound was sublimated at room temperature and deposited with a large excess of argon onto a CsI window (15 K). The IR spectrum of monomeric **TT** isolated in argon matrix is well reproduced by the B3LYP/6-311+G(2d,p) computed harmonic IR spectrum of the **s-OH-TT** hydroxy tautomeric form, except for some Fermi resonance and overtone bands appearing in the 1500–1250 cm⁻¹ region (Figure S5).⁵² A detailed assignment of this spectrum is provided in Table S1. Although **TT** was described to exist in solution and solid state as two

rapidly equilibrated hydroxy (**OH-TT**) and thiol (**SH-TT**) tautomeric structures,⁵³ the presence of thiol forms under matrix isolation conditions is excluded due to the lack of strong $\nu(\text{C}=\text{O})$ and other characteristic spectral features (Figure S6).⁵⁴ This picture is consistent with the relative energies computed for the most relevant isomers of **TT** (Table 1): **s-OH-TT** is the most stable form, followed by **s-SH-TT** (7.2–11.4 kJ mol⁻¹ higher in energy), while **a-OH-TT** and **a-SH-TT** are considerably more energetic (~55 and ~20 kJ mol⁻¹, respectively) since these forms do not bear the intramolecular hydrogen bond characteristic of the two most stable isomers (OH \cdots S=C in **s-OH-TT** or SH \cdots O=C in **a-SH-TT**). Accordingly, in the room temperature gas-phase equilibrium, **s-OH-TT** should strongly dominate ($\geq 96\%$).

Table 1. Relative Gibbs energy at 298.15 K ($\Delta G_{298\text{K}}$ in kJ mol⁻¹) computed at the CBS-QB3, MP2/6-311++G(3df,3pf), B2PLYP/6-311+G(2d,p) and B3LYP/6-311+G(2d,p) levels of theory for the four most relevant isomers of thiotropolone and their equilibrium populations at 298.15 K (Pop_{298K} in %).^{a,b}

Structure				
Name	s-OH-TT	a-OH-TT	s-SH-TT	a-SH-TT
CBS-QB3	0.0	51.6	7.5	17.1
MP2	0.0	55.9	11.4	24.3
B2PLYP	0.0	55.5	7.2	19.3
B3LYP	0.0	56.8	8.1	20.5
Pop _{298K}	96.3	0.0	3.7	0.0

^aEquilibrium populations were estimated from the Boltzmann distribution based on the B3LYP/6-311+G(2d,p) $\Delta G_{298\text{K}}$ values. ^bThe use of extended basis sets or dispersion correction has a minimal effect on the DFT relative energies (Table S3).

Because of the strong OH \cdots S=C H-bond, the $\nu(\text{OH})$ stretching mode of **s-OH-TT** [computed at 2688 cm⁻¹] originates a very broad absorption (barely noticeable) in the 2900–2400 cm⁻¹ range (Figure S7).^{55–58} The corresponding 2 $\nu(\text{OH})$ overtone [computed at 4916 cm⁻¹] was not detected in the near-IR spectrum. However, two bands were observed at 5980 and 5940 cm⁻¹ (Figure 1a). Based on B3LYP/6-311+G(2d,p) anharmonic computations, these bands were ascribed to overtone and combination bands of $\nu(\text{CH})$ modes (Figure 1b), whose fundamentals

appear near 3000 cm^{-1} (Figure S7). More details about the assigned overtones and combinations of $\nu(\text{CH})$ modes are given in Figure S8.

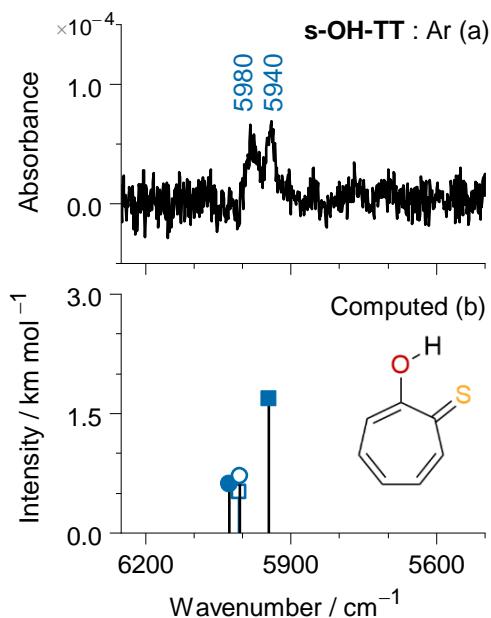


Figure 1. (a) Near-IR spectrum of the **s-OH-TT** form of thiotropolone in an argon matrix at 15 K. (b) Anharmonic wavenumbers and IR intensities of **s-OH-TT** computed at the B3LYP/6-311+G(2d,p) level of theory. Closed (\blacksquare) and open (\square) squares depict $2\nu_3(\text{CH})$ and $2\nu_5(\text{CH})$ overtone modes, respectively. Closed (\bullet) and open (\circ) circles depict $[\nu_3(\text{CH}) + \nu_2(\text{CH})]$ and $[\nu_5(\text{CH}) + \nu_4(\text{CH})]$ combination modes, respectively. Only overtone or combination modes with computed IR intensity $>0.4\text{ km mol}^{-1}$ are shown.

The effect of selective vibrational excitation of **s-OH-TT** was explored. Using narrowband light provided by an optical parametric oscillator, the matrix-isolated **s-OH-TT** was irradiated at 5980 and 5940 cm^{-1} , and the process followed by mid-IR spectroscopy (using a cut-off filter blocking IR light above 2200 cm^{-1}). Excitation at both frequencies was found to induce tautomerization of **s-OH-TT** into **a-SH-TT**. As shown in Figure 2a,b, the experimental difference IR spectrum is well reproduced by the B3LYP/6-311+G(2d,p) computed difference spectrum simulating this transformation. Some distinctive bands of **a-SH-TT** were observed at 1628, 1587, 1007, 770, and 563 cm^{-1} , corresponding to the vibrational modes computed at 1625 [$\nu_a(\text{C}=\text{C})$], 1586 [$\nu(\text{C}=\text{O})$], 1005 [$\nu_t(\text{C}-\text{C}) - \delta(\text{SH})$], 765 [$\tau_a(\text{ring}) - \gamma_e(\text{CH})$], and 556 cm^{-1} [$\nu(\text{C}-\text{S})$], respectively. A more detailed assignment is provided in Table S2. Although the

computed IR spectra of **a-SH-TT** and **s-SH-TT** are very similar, a detailed analysis of some spectral regions suggests the exclusive formation of **a-SH-TT** upon irradiation (Figure S9). As demonstrated below, **s-SH-TT** is expected to be a fleeting species that cannot be isolated or observed even at the cryogenic conditions of the performed experiments.

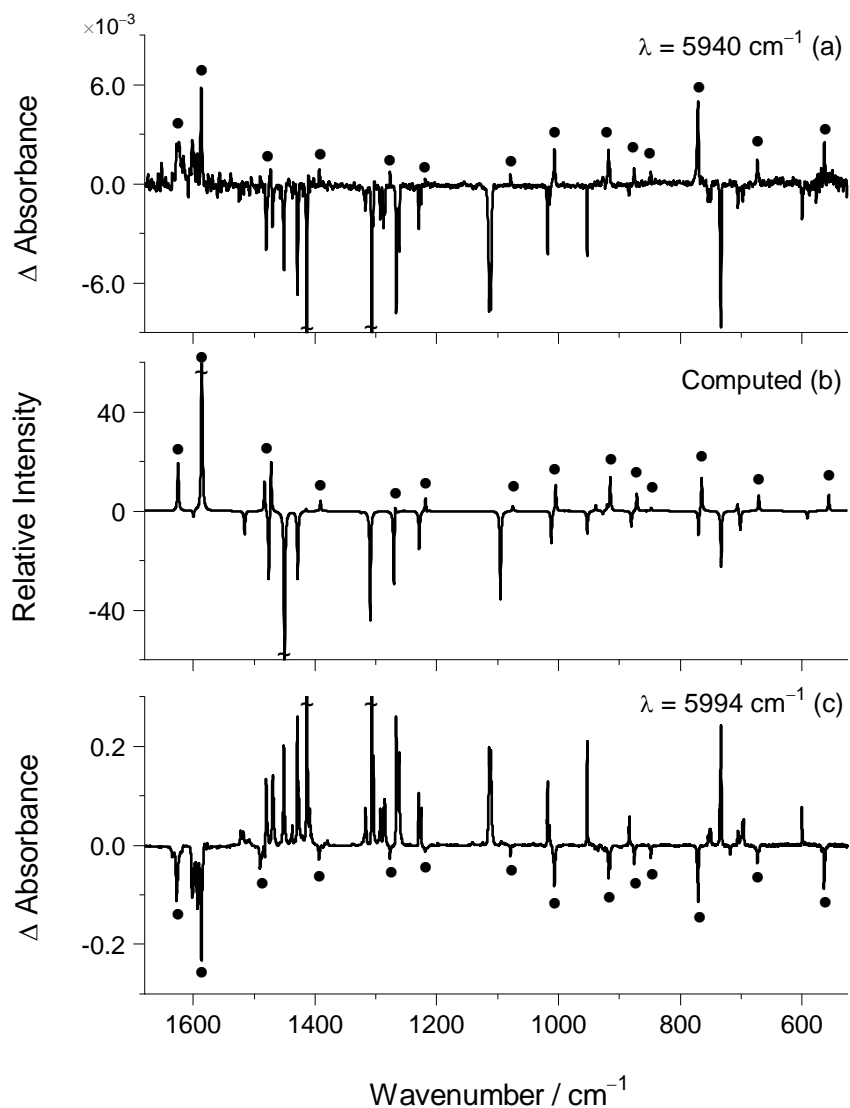


Figure 2. Experimental difference IR spectrum (spectrum after matrix irradiation “minus” spectrum of the same matrix before irradiation): (a) irradiation at $\lambda = 5940 \text{ cm}^{-1}$ (60 mW, 1 hour); (c) irradiation at $\lambda = 5994 \text{ cm}^{-1}$ (30 mW, 1 hour). Bands marked with circles (●) are due to **a-SH-TT**, which is produced by irradiation at $\lambda = 5940 \text{ cm}^{-1}$ (a) and consumed by irradiation at $\lambda = 5994 \text{ cm}^{-1}$ (c). (b) Simulated difference IR spectrum based on B3LYP/6-311+G(2d,p) vibrational data considering quantitative (1:1) transformation of **s-OH-TT** into **a-SH-TT**. The symbols of tilde (~) designate truncated bands.

After producing an argon matrix containing exclusively the **a-SH-TT** form (using irradiation at 440 nm, see SI for details), a near-IR spectrum was collected allowing the identification of two bands at 5994 and 5947 cm^{-1} (Figure S10a), ascribable to $\nu(\text{CH})$ overtone and combination modes (Figures S10b and S11). The sample was then irradiated at these wavenumbers, and tautomerization of **a-SH-TT** back to **s-OH-TT** was observed (Figure 2c). The experimental difference IR spectrum perfectly mirrors the inverse process of the transformation of **s-OH-TT** to **a-SH-TT** described above (Figure 2a,c). The only distinctive feature is that the **a-SH-TT** transformation into **s-OH-TT** occurs on a much larger scale.⁵⁹ These results demonstrate that the hydroxy/thiol tautomerization in **TT** is achieved in both directions by vibrational excitation at the $\nu(\text{CH})$ overtone or combination modes of the corresponding reactant tautomeric species (Scheme 2).

To rationalize the experimental observations, the potential energy surface (PES) profiles for tautomerization and rotamerizations of the most relevant isomers of **TT** (Figure 3) were computed. Upon excitation of **s-OH-TT** at 5980 or 5940 cm^{-1} , $\sim 71 \text{ kJ mol}^{-1}$ are introduced in the molecule. Such energy is below the transition state (TS) for OH-rotamerization ($\sim 76 \text{ kJ mol}^{-1}$) but well above the TS for tautomerization to **s-SH-TT** ($\sim 17 \text{ kJ mol}^{-1}$, as computed at the B3LYP/6-311+G(2d,p) level: for energies computed with other methods see Table S4). However, **s-SH-TT** should not persist and will promptly tautomerize back to **s-OH-TT** because of a low ($\sim 9 \text{ kJ mol}^{-1}$) and thin ($\sim 0.63 \text{ \AA}$) barrier (Figure S12). With such barrier, the occurrence of extremely fast quantum tunneling is expected, making **s-SH-TT** a fleeting species even at cryogenic conditions (estimated $\tau_{1/2} \sim 1 \times 10^{-11} \text{ s}$ applying the Wentzel–Kramers–Brillouin (WKB) model; see SI).^{60–66} Note, for instance, that the thiol \rightarrow thione tautomerization in thiourea has a much higher ($\sim 93 \text{ kJ mol}^{-1}$) and wider ($\sim 1.18 \text{ \AA}$) barrier (Figure S13), and even for that system, tunneling at cryogenic conditions was found to occur on a timescale of hours⁶⁷ (estimated $\tau_{1/2} \sim 5 \times 10^3 \text{ s}$, in fair agreement with experiment; see SI). These data unequivocally endorse the experimental capture and identification of thiol **a-SH-TT** (and not **s-SH-TT**) upon vibrational excitation of **s-OH-TT**. The formation of **a-SH-TT** has a barrier of $\sim 53 \text{ kJ mol}^{-1}$, clearly below the energy introduced in **s-OH-TT** upon vibrational excitation. The observed process shows that the excited $\nu(\text{CH})$ overtone/combination modes are coupled to some extent to the reaction coordinates for tautomerization and subsequent SH-rotamerization, leading to **a-SH-TT** through an IVR process crossing two reaction coordinates. The alternative occurrence

of a two-step process, involving the formation of a thermalized **s-SH-TT** at an intermediate stage, is unlikely, because **s-SH-TT** is expected to have both a very short lifetime and no significant bright transitions near 5980 or 5940 cm^{-1} (Table S6). Under these circumstances, the occurrence of vibrational excitation of **s-SH-TT** with subsequent activation of SH-rotamerization is impossible in practice.⁶⁸

The observed tautomerization of **a-SH-TT** back to **s-OH-TT** on a much larger scale is easier to conceptualize. Upon irradiation of **a-SH-TT** at 5990 or 5947 cm^{-1} , the vibrational energy deposited in the molecule ($\sim 71 \text{ kJ mol}^{-1}$) is high enough to activate SH-rotamerization to **s-SH-TT** ($\sim 33 \text{ kJ mol}^{-1}$ is required), which will rapidly tautomerize by tunneling to **s-OH-TT**. None of these phenomena (SH-rotamerization induced by vibrational excitation and thiol tautomerization by tunneling) is entirely unprecedented.^{26,67} It is also conceivable the existence of coupling between the excited $\nu(\text{CH})$ overtone/combination modes with the reaction coordinates for SH-rotamerization and subsequent tautomerization, allowing the direct formation of **s-OH-TT** from **a-SH-TT**, similarly to the process proposed for the opposite tautomerization.

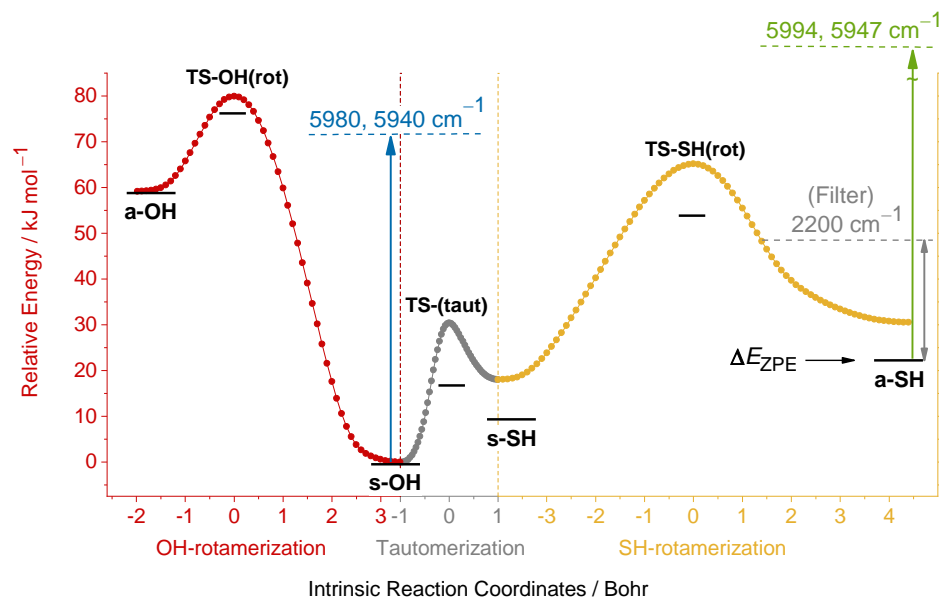


Figure 3. B3LYP/6-311+G(2d,p) computed intrinsic reaction coordinate (IRC) profiles for tautomerization (H-shift) and rotamerizations (OH- and SH-torsion) involving the most relevant isomers of thiotropolone. The horizontal bars at each stationary point (minima and transition states) show the corresponding computed ZPE-corrected relative energy value.

In conclusion, we demonstrated that bidirectional tautomerization of thiotropolone is achieved by vibrational excitation. The **s-OH-TT** \leftrightarrow **a-SH-TT** transformations involve

bond-breaking/bond-forming processes as result of vibrational excitation, which is a fascinating unprecedented observation. The observed processes also show that intramolecular vibrational redistribution in **TT** can transport energy deposited in the CH stretching overtone or combination modes towards the distant reaction coordinates leading to the hydroxy \leftrightarrow thiol tautomerizations. These pioneer results of a bond-breaking/bond-forming reaction activated by vibrational excitation under matrix-isolation conditions can be expected to lead to new exciting advances in vibrationally induced chemistry.

ASSOCIATED CONTENT

Supporting Information. The Supporting Information is available free of charge on the ACS Publications website at DOI: xxx.xxx.xxx. Experimental and computational procedures, additional experimental results, vibrational assignments, and computational data.

Author Emails. cmnunes@qui.uc.pt, npereira@qui.uc.pt, reva@qui.uc.pt, patricia.s.amado@gmail.com, mcristi@ualg.pt, rfausto@ci.uc.pt

AUTHOR INFORMATION

Corresponding Author

*cmnunes@qui.uc.pt

Author Contributions

C.M.N. conceived the original working hypothesis and wrote the first draft of the manuscript. C.M.N. and N.A.M.P. performed the experiments. C.M.N., N.A.M.P., I.R. and R.F. performed the computations and analyzed the data. P.S.M.A. and M.L.S.C. performed the synthesis. All authors discussed and co-wrote the final version of the manuscript.

Notes

The authors declare no competing interests.

ACKNOWLEDGMENT

This work was supported by Project POCI-01-0145-FEDER-028973, funded by FEDER, via Portugal 2020 - POCI, and by National Funds via the Portuguese Foundation for Science and Technology (FCT). The Coimbra Chemistry Centre and the Center of Marine Sciences (CCMar) are supported by FCT through projects UIDB/QUI/0313/2020, UIDP/QUI/0313/2020 and UID/MULTI/04326/2019, cofunded by COMPETE. C.M.N. acknowledges FCT for an Auxiliary Researcher grant. N.A.M.P acknowledges the Project POCI-01-0145-FEDER-028973 for a Junior Researcher grant. P.S.M.A. acknowledges FCT for Grant SFRH/BD/130407/2017

REFERENCES

- (1) Thomas, A.; Nagarajan, K.; Vergauwe, R. M. A.; George, J.; Chervy, T.; Shalabney, A.; Devaux, E.; Genet, C.; Moran, J.; Ebbesen, T. W. Tilting a ground-state reactivity landscape by vibrational strong coupling. *Science* **2019**, *363*, 615–619.
- (2) Rafiq, S.; Bezdek, M. J.; Chirik, P. J.; Scholes, G. D. Dinitrogen coupling to a terpyridine-molybdenum chromophore is switched on by fermi resonance. *Chem* **2019**, *5*, 402–416.
- (3) Heyne, K.; Kühn, O. Infrared laser excitation controlled reaction acceleration in the electronic ground state. *J. Am. Chem. Soc.* **2019**, *141*, 11730–11738.
- (4) Crim, F. F. Chemical dynamics of vibrationally excited molecules: Controlling reactions in gases and on surfaces. *Proc. Natl. Acad. Sci. U. S. A.* **2008**, *105*, 12654–12661, and references cited herein.
- (5) Gruebele, M.; Wolynes, P. G. Vibrational energy flow and chemical reactions. *Acc. Chem. Res.* **2004**, *37*, 261–267.
- (6) Crim, F. F. Vibrational state control of bimolecular reactions: Discovering and directing the chemistry. *Acc. Chem. Res.* **1999**, *32*, 877–884.
- (7) Crim, F. F. State- and bond-selected unimolecular reactions. *Science* **1990**, *249*, 1387–1392.
- (8) Windhorn, L.; Yeston, J. S.; Witte, T.; Fuß, W.; Motzkus, M.; Proch, D.; Kompa, K. L.; Moore, C. B. Getting ahead of IVR: A demonstration of mid-infrared induced molecular dissociation on a sub-statistical time scale. *J. Chem. Phys.* **2003**, *119*, 641–645.

- (9) Boyall, D.; Reid, K. Intramolecular vibrational energy redistribution. *Chem. Soc. Rev.* **1997**, *26*, 223–232.
- (10) Karmakar, S.; Keshavamurthy, S. Intramolecular vibrational energy redistribution and the quantum ergodicity transition: A phase space perspective. *Phys. Chem. Chem. Phys.* **2020**, *22*, 11139–11173.
- (11) Liu, F.; Beames, J. M.; Petit, A. S.; McCoy, A. B.; Lester, M. I. Infrared-driven unimolecular reaction of CH₃CHOO Criegee intermediates to OH radical products. *Science* **2014**, *345*, 1596–1598.
- (12) Other landmark is the recently reported acceleration of urethane and polyurethane formation in solution by vibrational excitation at the OH and NCO stretching of their alcohol and isocyanate reactants, respectively, see ref. 13. For the first case of a vibrationally driven bimolecular reaction in solution, see ref 14.
- (13) Stensitzki, T.; Yang, Y.; Kozich, V.; Ahmed, A. A.; Kössl, F.; Kühn, O.; Heyne, K. Acceleration of a ground-state reaction by selective femtosecond-infrared-laser-pulse excitation. *Nat. Chem.* **2018**, *10*, 126–131.
- (14) Shin, J. Y.; Shaloski, M. A.; Crim, F. F.; Case, A. S. First evidence of vibrationally driven bimolecular reactions in solution: Reactions of Br atoms with dimethylsulfoxide and methanol. *J. Phys. Chem. B* **2017**, *121*, 2486–2494.
- (15) Dzugan, L. C.; Matthews, J.; Sinha, A.; McCoy, A. B. Role of torsion-vibration coupling in the overtone spectrum and vibrationally mediated photochemistry of CH₃OOH and HOOH. *J. Phys. Chem. A* **2017**, *121*, 9262–9274.
- (16) Matthews, J.; Fry, J. L.; Roehl, C. M.; Wennberg, P. O.; Sinha, A. Vibrational overtone initiated unimolecular dissociation of HOCH₂OOH and HOCD₂OOH: Evidence for mode selective behavior. *J. Chem. Phys.* **2008**, *128*, 1–13.
- (17) Grinevich, O.; Snavely, D. L. Laser vibrational overtone activation of ethyl acrylate/benzoyl peroxide mixture. *Chem. Phys. Lett.* **1999**, *304*, 202–206.
- (18) Leytner, S.; Snavely, D. L.; Grinevich, O. Reversible isomerization of methylcyclopentadienes directed by selective excitation of the methyl out-of-plane fourth overtone transition. *Chem. Phys. Lett.* **1997**, *277*, 443–449.
- (19) Snavely, D. L.; Grinevich, O.; Hassoon, S.; Snavely, G. Vibrational overtone activation of

- methylcyclopropene. *J. Chem. Phys.* **1996**, *104*, 5845–5851.
- (20) Hassoon, S.; Rajapakse, N.; Snively, D. L. Vibrational overtone activation of the isomerization of methyl isocyanide. *J. Phys. Chem.* **1992**, *96*, 2576–2581.
- (21) Lishan, D. G.; Reddy, K. V.; Hammond, G. S.; Leonard, J. E. Overtone vibrational photochemistry of quadricyclane. *J. Phys. Chem.* **1988**, *92*, 656–660.
- (22) Benmair, R. M. J.; Yogev, A. I.R. laser chemistry of allyl phenyl ether. *Mol. Phys.* **1987**, *60*, 717–724.
- (23) Schwebel, A.; Brestel, M.; Yogev, A. Site-selective liquid-phase vibrational overtone photochemistry of hydroxyhexadiene. *Chem. Phys. Lett.* **1984**, *107*, 579–584.
- (24) Jasinski, J. M.; Frisoli, J. K.; Moore, C. B. High vibrational overtone photochemistry of 1-cyclopropylcyclobutene. *J. Chem. Phys.* **1983**, *79*, 3826–3829.
- (25) Fausto, R.; Khriachtchev, L.; Hamm, P. Conformational Changes in Cryogenic Matrices. In *Physics and Chemistry at Low Temperatures*; Khriachtchev, L., Ed.; Pan Stanford Publishing: United States, 2011; pp 51–84.
- (26) Góbi, S.; Reva, I.; Csonka, I. P.; M. Nunes, C.; Tarczay, G.; Fausto, R. Selective conformational control by excitation of NH imino vibrational antennas. *Phys. Chem. Chem. Phys.* **2019**, *21*, 24935–24949.
- (27) Lopes Jesus, A. J.; Nunes, C. M.; Reva, I.; Pinto, S. M. V.; Fausto, R. Effects of entangled IR radiation and tunneling on the conformational interconversion of 2-cyanophenol. *J. Phys. Chem. A* **2019**, *123*, 4396–4405.
- (28) Lopes Jesus, A. J.; Nunes, C. M.; Fausto, R.; Reva, I. Conformational control over an aldehyde fragment by selective vibrational excitation of interchangeable remote antennas. *Chem. Commun.* **2018**, *54*, 4778–4781.
- (29) Ryazantsev, S. V.; Feldman, V. I.; Khriachtchev, L. Conformational switching of HOCO radical: Selective vibrational excitation and hydrogen-atom tunneling. *J. Am. Chem. Soc.* **2017**, *139*, 9551–9557.
- (30) Duvernay, F.; Butscher, T.; Chiavassa, T.; Coussan, S. IR induced photochemistry of glycolaldehyde in nitrogen matrix. *Chem. Phys.* **2017**, *496*, 9–14.
- (31) Coussan, S.; Tarczay, G. Infrared laser induced conformational and structural changes of glycine and glycine·water complex in low-temperature matrices. *Chem. Phys. Lett.* **2016**, *644*, 189–194.

- (32) Halasa, A.; Reva, I.; Lapinski, L.; Rostkowska, H.; Fausto, R.; Nowak, M. J. Conformers of kojic acid and their near-IR-induced conversions: Long-range intramolecular vibrational energy transfer. *J. Phys. Chem. A* **2016**, *120*, 2647–2656.
- (33) Halasa, A.; Lapinski, L.; Rostkowska, H.; Nowak, M. J. Intramolecular vibrational energy redistribution in 2-thiocytosine: SH rotamerization induced by near-IR selective excitation of NH₂ stretching overtone. *J. Phys. Chem. A* **2015**, *119*, 9262–9271.
- (34) Reva, I.; Nunes, C. M.; Biczysko, M.; Fausto, R. Conformational switching in pyruvic acid isolated in Ar and N₂ matrixes: Spectroscopic analysis, anharmonic simulation, and tunneling. *J. Phys. Chem. A* **2015**, *119*, 2614–2627.
- (35) Lopes Jesus, A. J.; Reva, I.; Araujo-Andrade, C.; Fausto, R. Conformational switching by vibrational excitation of a remote NH bond. *J. Am. Chem. Soc.* **2015**, *137*, 14240–14243.
- (36) Najbauer, E. E.; Bazsó, G.; Góbi, S.; Magyarfalvi, G.; Tarczay, G. Exploring the conformational space of cysteine by matrix isolation spectroscopy combined with near-infrared laser induced conformational change. *J. Phys. Chem. B* **2014**, *118*, 2093–2103.
- (37) Nunes, C. M.; Lapinski, L.; Fausto, R.; Reva, I. Near-IR laser generation of a high-energy conformer of L-alanine and the mechanism of its decay in a low-temperature nitrogen matrix. *J. Chem. Phys.* **2013**, *138*, 125101.
- (38) Bazsó, G.; Najbauer, E. E.; Magyarfalvi, G.; Tarczay, G. Near-infrared laser induced conformational change of alanine in low-temperature matrixes and the tunneling lifetime of its conformer VI. *J. Phys. Chem. A* **2013**, *117*, 1952–1962.
- (39) Wassermann, T. N.; Suhm, M. A.; Roubin, P.; Coussan, S. Isomerization around C–C and C–O bonds in 1-propanol: Collisional relaxation in supersonic jets and selective IR photo-isomerization in cryogenic matrices. *J. Mol. Struct.* **2012**, *1025*, 20–32.
- (40) Bazsó, G.; Magyarfalvi, G.; Tarczay, G. Tunneling lifetime of the Ttc/VIp conformer of glycine in low-temperature matrices. *J. Phys. Chem. A* **2012**, *116*, 10539–10547.
- (41) Lapinski, L.; Nowak, M. J.; Reva, I.; Rostkowska, H.; Fausto, R. NIR-laser-induced selective rotamerization of hydroxy conformers of cytosine. *Phys. Chem. Chem. Phys.* **2010**, *12*, 9615–9618.
- (42) Sharma, A.; Reva, I.; Fausto, R. Conformational switching induced by near-infrared laser irradiation. *J. Am. Chem. Soc.* **2009**, *131*, 8752–8753.
- (43) Khriachtchev, L. Rotational isomers of small molecules in noble-gas solids: From

- monomers to hydrogen-bonded complexes. *J. Mol. Struct.* **2008**, 880, 14–22.
- (44) Dian, B. C.; Longarte, A.; Zwier, T. S. Conformational dynamics in a dipeptide after single-mode vibrational excitation. *Science* **2002**, 296, 2369–2373.
- (45) Pettersson, M.; Lundell, J.; Khriachtchev, L.; Rasanen, M. IR spectrum of the other rotamer of formic acid, cis-HCOOH. *J. Am. Chem. Soc.* **1997**, 119, 11715–11716.
- (46) It was recently demonstrated that selective conformational isomerizations can also be achieved using excitation to second stretching overtones See: Nunes, C. M.; Reva, I.; Fausto, R. Conformational isomerizations triggered by vibrational excitation of second stretching overtones. *Phys. Chem. Chem. Phys.* **2019**, 21, 24993–25001.
- (47) We have recently reported a heavy-atom tunneling event involving the ring expansion of a fused-ring benzazirine into a seven-membered ring ketenimine. Interestingly, broadband IR radiation, from the spectrometer globar, was found to increase the rate of this transformation, which may indicate that the reaction is also promoted by vibrational excitation. See: Nunes, C. M.; Reva, I.; Kozuch, S.; McMahon, R. J.; Fausto, R. photochemistry of 2-formylphenylnitrene: A doorway to heavy-atom tunneling of a benzazirine to a cyclic ketenimine. *J. Am. Chem. Soc.* **2017**, 139, 17649–17659.
- (48) Catalano and Barletta also tentatively reported a bimolecular reaction between SF₆ and nitrogen oxides induced by vibrational excitation under matrix isolation conditions. However, no product assignments could be made to show conclusively that IR laser-induced photochemistry is really occurring. See: Catalano, E.; Barletta, R. E. Infrared laser single photon absorption reaction chemistry in the solid state. Reactions of nitrogen oxides with sulfur hexafluoride. *J. Phys. Chem.* **1980**, 84, 1686–1694.
- (49) Frei, H.; Fredin, L.; Pimentel, G. C. Vibrational excitation of ozone and molecular fluorine reactions in cryogenic matrices. *J. Chem. Phys.* **1981**, 74, 397–411.
- (50) Cesaro, S. N.; Frei, H.; Pimentel, G. C. Vibrational excitation of the reaction between vinyl bromide and fluorine in solid argon. *J. Phys. Chem.* **1983**, 87, 2142–2147.
- (51) Knudsen, A. K.; Pimentel, G. C. Vibrational excitation of the allene-fluorine reaction in cryogenic matrices: Possible mode selectivity. *J. Chem. Phys.* **1983**, 78, 6780–6792.
- (52) The IR spectrum of matrix-isolated tropolone, a structurally similar species, also shows significant complexity in 1650–1400 cm⁻¹ region due to existence of Fermi resonances and overtone bands. See: Redington, R. L.; Redington, T. E.; Montgomery, J. M. IR

- spectra of tropolone(OH) and tropolone(OD). *J. Chem. Phys.* **2000**, *113*, 2304–2318.
- (53) Machiguchi, T.; Hasegawa, T.; Saitoh, H.; Yamabe, S.; Yamazaki, S. Solid-state thiotropolone: An extremely rapid intramolecular proton transfer. *J. Org. Chem.* **2011**, *76*, 5457–5460.
- (54) The possibility of H-atom tunneling from **OH-TT** to **SH-TT** was clearly ruled out at low-temperatures. See: Fernández-Ramos, A. Correct interpretation of how tunneling proceeds at low temperatures in the proton transfer reactions involving thiotropolone: A comment. *Angew. Chemie - Int. Ed.* **2013**, *52*, 8204–8205.
- (55) Similar effect was observed for other molecules with a strong OH···X (X = S, O or N) intramolecular H-bond, see for instance refs. 56–58.
- (56) Liu, Z. Y.; Hu, J.-W.; Huang, C.-H.; Huang, T.-H.; Chen, D.-G.; Ho, S.-Y.; Chen, K.-Y.; Li, E. Y.; Chou, P.-T. Sulfur-based intramolecular hydrogen-bond: Excited-state hydrogen-bond on/off switch with dual room-temperature phosphorescence. *J. Am. Chem. Soc.* **2019**, *141*, 9885–9894.
- (57) Rostkowska, H.; Nowak, M. J.; Lapinski, L.; Adamowicz, L. IR spectral and theoretical characterization of intramolecular hydrogen bonds closing five-membered rings. *Phys. Chem. Chem. Phys.* **2001**, *3*, 3012–3017.
- (58) Duarte, L.; Giuliano, B.M.; Reva, I.; Fausto, R. Tautomers and UV-induced photoisomerization of a strongly intramolecularly H-bonded aromatic azo-dye: 1-(Cyclopropyl)diazo-2-naphthol. *J. Phys. Chem. A* **2013**, *117*, 10671-10680.
- (59) Regarding the IR irradiation conditions mentioned in Figure 2, the ratio of the **a-SH-TT** → **s-OH-TT** transformation exceeded 60% whereas the proportion of **s-OH-TT** → **a-SH-TT** transformation was of a few percent only.
- (60) A structure corresponding to a local minimum on the PES is not sufficient condition to be a stable observable molecule at cryogenic temperature. The possibility of spontaneous tunneling needs to be considered. See refs. 61 and 62.
- (61) Hoffmann, R.; Schleyer, P. V. R.; Schaefer, H. F. Predicting molecules - more realism, please! *Angew. Chemie - Int. Ed.* **2008**, *47*, 7164–7167.
- (62) Kozuch, S. A Quantum mechanical jack in the box: Rapid rearrangement of a tetrahedryl-tetrahedrane via heavy atom tunneling. *Org. Lett.* **2014**, *16*, 4102–4105.
- (63) The WKB model has been successfully used to rationalize tunneling reactions observed in

cryogenic matrix, see for instance refs. 64–66.

- (64) Góbi, S.; Nunes, C. M.; Reva, I.; Tarczay, G.; Fausto, R. S-H rotamerization *via* tunneling in a thiol form of thioacetamide. *Phys. Chem. Chem. Phys.* **2019**, *21*, 17063–17071.
- (65) Nunes, C. M.; Knezz, S. N.; Reva, I.; Fausto, R.; McMahon, R. J. Evidence of a nitrene tunneling reaction: Spontaneous rearrangement of 2-formyl phenylnitrene to an imino ketene in low-temperature matrixes. *J. Am. Chem. Soc.* **2016**, *138*, 15287–15290.
- (66) C. M. Nunes, I. Reva, R. Fausto, *Direct Observation of Tunneling Reactions by Matrix Isolation Spectroscopy*. In "Tunnelling in Molecules: Nuclear Quantum Effects from Bio to Physical Chemistry"; S. Kozuch and J. Kästner, Eds.; RSC, 2020; in press.
- (67) Rostkowska, H.; Lapinski, L.; Nowak, M. J. Hydrogen-atom tunneling through a very high barrier; spontaneous thiol → thione conversion in thiourea isolated in low-temperature Ar, Ne, H₂ and D₂ matrices. *Phys. Chem. Chem. Phys.* **2018**, *20*, 13994–14002.
- (68) Note that our laser system operates at 10 Hz, meaning a laser pulse each 0.1 s.

Supporting Information

Bond-Breaking/Bond-Forming Reactions by Vibrational Excitation: Infrared-Induced Bidirectional Tautomerization of Matrix-Isolated Thiotropolone

Cláudio M. Nunes,^{1*} Nelson A. M. Pereira,¹ Igor Reva,¹ Patrícia S. M. Amado,² Maria L. S. Cristiano,² and Rui Fausto¹

¹University of Coimbra, CQC, Department of Chemistry, 3004-535 Coimbra, Portugal

²Center of Marine Sciences, CCMAR, and Department of Chemistry and Pharmacy, University of Algarve, 8005-139 Faro, Portugal

Email: *cmnunes@qui.uc.pt, npereira@qui.uc.pt, reva@qui.uc.pt, patricia.s.amado@gmail.com, mcristi@ualg.pt, rfausto@ci.uc.pt

Table of contents

1.	Experimental and Computational Methods	S2
2.	Figures	S6
2.1	NMR and Mass Spectra of 2-Tolylsulfonyloxytropone and Thiotropolone	S6
2.2	2.2 IR Spectra and IRC graphs	S9
3.	Tables	S18
3.1	Vibrational Data	S18
3.2	Computed Energies	S22
4.	References	S28

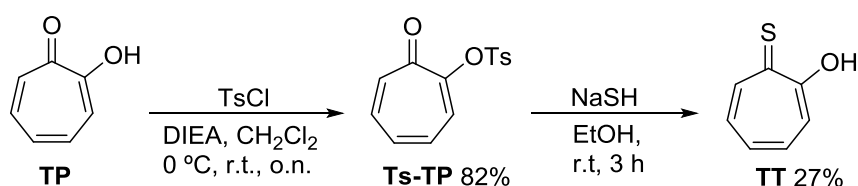
1. Experimental and Computational Methods

1.1 General

Commercial reagents were used as purchased. ^1H and ^{13}C Nuclear Magnetic Resonance (NMR) spectra were recorded on an NMR spectrometer Bruker Avance III operating at 400 and 100 MHz, respectively. ^1H NMR chemical shifts are referred to the residual signal of CDCl_3 (δ_{H} 7.26) and ^{13}C NMR chemical shifts to the CDCl_3 signal (δ_{C} 77.0), or to the internal standard tetramethylsilane (TMS). Chemical shifts are given in parts per million (ppm) relative to TMS and coupling constants J are given in Hertz. Thin-layer chromatography (TLC) was carried out on silica gel 60 F₂₅₄ plates (AL TLC 20x20). Column chromatography was performed on Silica Gel 60 (0.04 - 0.063 mm). Melting points ($^{\circ}\text{C}$) were obtained on an SMP3 melting point apparatus and are uncorrected. High-resolution mass spectrometry (HRMS) was conducted on an Agilent QTOF 7200 spectrometer, for chemical ionisation (CI), or on an Agilent QTOF 6540 spectrometer, for electrospray ionization (ESI).

1.2 Synthesis

The synthesis of thiotropolone (**TT**) was carried out by adapting the methodology described by Elagawany *et al.*^{S1} for the preparation of 4-isopropyl-thiotropolone, with slight modifications (Scheme S1).



Scheme S1. Preparation of thiotropolone (**TT**)

2-Tolylsulfonyloxypone (**Ts-TP**)^{S2}

Tropolone (**TP**, 1.5 g, 12.3 mmol) and *N,N*-diisopropylethylamine (DIEA) (4.3 mL, 24.5 mmol) were dissolved in dichloromethane (50 mL), the solution was cooled to 0 $^{\circ}\text{C}$ and then *p*-toluenesulfonyl chloride (2.57 g, 13.48 mmol) was added. The mixture was left to warm to room temperature and stirred overnight. The final mixture was washed with 1 M HCl (30 mL), water (2 x 30 mL) and brine (30 mL). The organic layer was dried over MgSO_4 , filtered and the solvent was evaporated to dryness under reduced pressure. Crystallization of the crude product from ethanol gave the desired compound **Ts-TP** in 82% yield (2.8 g, 10.1 mmol) as a brown solid (m.p. 158–159 $^{\circ}\text{C}$). Spectral data are in accordance with the reported in the literature.^{S2}

^1H NMR (CDCl_3) δ 7.92 (d, J = 8.4 Hz, 2H), 7.43 (dd, J = 9.4, 0.9 Hz, 1H), 7.35 (d, J = 8.1 Hz, 2H), 7.22 (ddd, J = 12.3, 7.9, 1.2 Hz, 1H), 7.15 (m, 1H), 7.09 (m, 1H), 6.98 (m, 1H), 2.45 (s, 3H). ^{13}C NMR (CDCl_3) δ 179.42, 155.14, 145.55, 141.20, 136.41, 134.71, 133.40, 130.83, 129.99, 129.64, 128.58, 21.77. HRMS (ESI⁺, m/z) calcd for $\text{C}_{14}\text{H}_{12}\text{O}_4\text{SNa}$ ($\text{M}+\text{Na}$)⁺: 299.0349, found 299.0352.

Thiotropolone (TT)^{S3}

NaSH (1.2 g, 21.7 mmol) was added to a solution of **Ts-TP** (1.5 g, 5.4 mmol) in ethanol (100 mL). The reaction mixture was stirred for 3 h at room temperature and was monitored by TLC till completion. Then, the solvent was evaporated and the resulting solid was dissolved in water and acidified with HCl (2 M), then extracted with dichloromethane (3 x 30 mL). The combined organic layers were dried over MgSO₄, filtered and the solvent was evaporated under reduced pressure, giving a red oily residue. Purification by sublimation *in vacuo* at 80 °C gave the pure compound **TT** (202 mg, 27%) as a bright orange solid (m.p. 54-55 °C, lit.^{S3} 54-55 °C). Spectral data are in accordance with the reported in the literature.^{S3}

¹H NMR (CDCl₃-*d*): δ 9.94 (s, 1H), 8.53 (m, 1H), 7.46 (m, 1H), 7.38 (m, 1H), 7.27 (m, 1H), 7.22 (d, *J* = 10.8 Hz, 1H). ¹³C NMR (CDCl₃-*d*): δ 183.37, 173.91, 143.58, 137.99, 133.98, 133.02, 120.49. HRMS (CI⁺, *m/z*) calcd for C₇H₇OS (M+H)⁺: 139.0212, found 139.0213.

1.3 Matrix Isolation Spectroscopy

In the matrix-isolation experiments, a CsI window mounted on the cryostat and used as optical substrate was maintained at low temperature by a closed-cycle helium refrigerator (APD Cryogenics, with a DE-202A expander). The temperature of the window was measured directly at its holder by a silicon diode sensor connected to a digital controller (Scientific Instruments, Model 9650-1). Infrared (IR) spectra were recorded using a Thermo Nicolet 6700 Fourier-transform infrared spectrometer (FTIR), purged through the optical path with dry air to avoid interference of atmospheric H₂O and CO₂. A deuterated triglycine sulfate detector (DTGS) and a KBr beam splitter were used to collect spectra with 0.5 cm⁻¹ resolution in the mid-IR region (4000 – 400 cm⁻¹). In the near-IR range (7500 – 4000 cm⁻¹) the spectra were acquired with a resolution of 2 cm⁻¹ using a thermoelectrically cooled indium gallium arsenide detector (InGaAs) and a CaF₂ beam splitter. In some cases, a cut-off filter (standard Edmund Optics long-pass filter) was applied to ensure that the matrix was not exposed to light from the FTIR spectrometer source with wavenumbers above 2200 cm⁻¹.

For the deposition of **TT**, a glass tube containing a small amount of the solid sample was connected to a needle valve (SS4 BMRG valve, NUPRO) linked to the vacuum chamber of the cryostat. The system was pumped, prior to lowering the temperature, to remove any volatile impurities. Low-temperature matrices were then obtained by co-deposition of the sample, sublimated at room temperature in vacuum (residual pressure *ca.* 10⁻⁶ mbar), with a large excess of argon (N60, Air Liquide) onto the CsI window at 15 K.

1.4 Irradiation Experiments

The matrix-isolated **s-OH-TT** and **a-SH-TT** forms were irradiated at the frequencies of their $\nu(\text{CH})$ overtones/combination bands, as described in the main text, using tunable narrowband (~0.2 cm⁻¹ spectral width) near-IR light generated by the idler beam of a Quanta-Ray MOPO-SL optical parametric oscillator (OPO), pumped by a pulsed Nd:YAG laser (pulse duration: 10 ns; repetition rate: 10 Hz). An argon matrix containing only the **s-OH-TT** form was produced by a direct deposition of **TT**, as described in section 1.3 (see also the main text). An argon matrix containing only the **a-SH-TT** form was produced by irradiation of the deposited **s-OH-TT** form (~100% conversion) with visible light at 440 nm (5mW, 10 min). For irradiations in the visible range the signal beam of the laser/OPO system was used. Note that a generalized heating process cannot be responsible for the observed hydroxy/thiol tautomerizations of **TT** (in any direction, **s-OH-TT** → **a-SH-TT** or **a-SH-TT** → **s-OH-TT**),

which occur upon vibrational excitation of the $\nu(\text{CH})$ overtone or combination modes of the corresponding reactant tautomeric species (see main text). In fact, overcoming the tautomerization energy barriers (see Figure 3) *via* a conventional thermal process would require temperatures well-above 40 K and, consequently, the destruction of the matrix (solid argon sublimates at about this temperature). We did not observe any changes in the vacuum pressure (baseline pressure was always $\sim 10^{-6}$ mbar) or any evidence of aggregation in the IR spectra during the infrared-induced tautomerizations processes (the argon matrix was kept intact and no molecular diffusion was taking place). Moreover, we did not observe any evidence of tautomerization upon annealing either an **s-OH-TT** or an **a-SH-TT** argon matrix up to 40 K (in separate experiments).

1.5 Theoretical Computations

All quantum chemical computations were carried out using the Gaussian 16 software package.^{S4} Geometry optimizations were performed at different levels of theory: density-functional theory (DFT) computations using the B2PLYP^{S5} and B3LYP^{S6-S9} functionals, second-order Møller-Plesset perturbation theory (MP2)^{S10} and complete basis set (CBS-QB3)^{S11} methods. The 6-311++G(3df,3pd) and 6-311+G(2d,p) basis sets were used in the DFT and MP2 calculations, and the influence of empirical dispersion with Becke Johnson damping (GD3BJ)^{S12} was also assessed for the B2PLYP and B3LYP methods. Harmonic vibrational frequencies were calculated at each level of theory and the nature of the stationary points, resulting from the optimizations, was confirmed by the analysis of the corresponding Hessian matrices. Gibbs energies obtained from the computations were used to estimate the equilibrium Boltzmann populations of the most relevant isomers of thiotropolone at 298.15 K. The potential energy surfaces along the rotamerization and tautomerization reaction paths were computed at the B3LYP/6-311+G(2d,p) level by following intrinsic reaction coordinate (IRC)^{S13} in both directions.

To support the interpretation of the experimental mid-IR spectra, harmonic frequency computations were performed at the B3LYP/6-311+G(2d,p) level of theory. The obtained harmonic vibrational frequencies were scaled by a factor of 0.979 based on our previous work.^{S14} The resulting frequencies, together with the calculated infrared intensities were used to simulate the IR spectra by convoluting each peak with a Lorentzian function (FWHM = 2 cm^{-1}). The integral band intensities correspond to the calculated infrared absolute intensities are presented in the arbitrary units of “Relative Intensity”. To support the interpretation of the experimental near-IR spectra, anharmonic frequency computations were performed at the B3LYP/6-311+G(2d,p) level of theory using the generalized second-order perturbation theory (GVPT2)^{S15,S16} as implemented in Gaussian 16. To ensure accuracy of the results, these computations were performed using the very tight optimization criteria and the superfine integration grid. The molecular vibrations of **TT** computed at the B3LYP/6-311+G(2d,p) level were subjected to the VMARD (Vibrational Mode Automatic Relevance Determination) analysis using Bayesian regression, as recently defined by Teixeira and Cordeiro.^{S17} The results of this analysis for the fundamental $\nu(\text{CH})$ stretching modes are shown in Figure S8 (for **s-OH-TT**) and Figure S11 (for **a-SH-TT**).

1.6 Tunneling Computations

For tunneling computations we used B3LYP/6-311+G(2d,p) computed potential energy profiles along the IRC, calculated in non-mass-weighted Cartesian coordinates expressed in units of Bohr. The transmission coefficients of the H-atom tunneling through a parabolic

barrier were estimated using the Wentzel–Kramers–Brillouin (WKB) approximation.^{S18–S20} According to this model, the probability $P(E)$ of tunneling can be written:

$$P(E) = e^{-\pi^2 w \sqrt{2m(V_0 - E)}/h}$$

where a particle with mass m tunnels through a barrier with height V_0 and width w , $(V_0 - E)$ is the energy deficiency of the particle with respect to the top of the barrier, and h is the Planck's constant. We applied this model to the following reactions:

(i) Tautomerization tunneling of thiotropolone **s-SH-TT** to **s-OH-TT**:

Using the calculated barrier height of 8.9 kJ mol⁻¹ and width at the ZPE level of 1.18 Bohr (equivalent of 0.624 Å, see Figure S12), the probability of tunneling (transmission coefficient) for tautomerization of **s-SH-TT** to **s-OH-TT** is estimated to be 1.5×10^{-3} . The tunneling rate is a product of the transmission coefficient and the frequency of attempts. In this model calculation, if the light H-atom of the thiol group of **s-SH-TT** is vibrating at an SH stretching frequency of about 2386.4 cm⁻¹ (B3LYP/6-311+G(2d,p) anharmonic computed value), it results in a tunneling rate of 1.1×10^{11} s⁻¹, i.e. a half-life time of 6.5×10^{-12} s. Alternatively, assuming that the vibrational movement responsible for the H-atom tunneling is not the ν SH stretching, but rather the δ CCS(H) bending mode (B3LYP/6-311+G(2d,p) anharmonic computed frequency equal to 258.8 cm⁻¹, which is the lowest-frequency mode of the A' symmetry in **s-SH-TT**), then we obtain (with the same transmission coefficient as above) a tunneling rate of 1.2×10^{10} s⁻¹, and a half-life time of 6.0×10^{-11} s.

(ii) Tautomerization tunneling of thiourea thiol **SH-TU** to thione **S-TU**:

Using the calculated barrier height of 93.2 kJ mol⁻¹ and width at the ZPE level of 2.23 Bohr (equivalent of 1.180 Å, see Figure S13), the probability of tunneling (transmission coefficient) for tautomerization of **SH-TU** to **S-TU** is estimated to be 6.4×10^{-18} . The tunneling rate is a product of the transmission coefficient and the frequency of attempts. In this model calculation, if the light H-atom of the thiol group of **SH-TU** is vibrating at an SH stretching frequency of about 2583.5 cm⁻¹ (B3LYP/6-311+G(2d,p) anharmonic computed value) it results in a tunneling rate of 5.0×10^{-4} s⁻¹, i.e. a half-life time of 1.4×10^3 s. Alternatively, assuming that the vibrational movement responsible for the H-atom tunneling is not the ν SH stretching, but rather the δ NCS(H) bending mode (anharmonic B3LYP/6-311+G(2d,p) computed frequency equal to 373.8 cm⁻¹), then we obtain (with the same transmission coefficient as above) a tunneling rate of 7.2×10^{-5} s⁻¹, i.e. a half-life time of 9.7×10^3 s.

2. Figures

2.1 ^1H and ^{13}C NMR and Mass Spectra of 2-Tolylsulfonyloxypone and Thiotropone

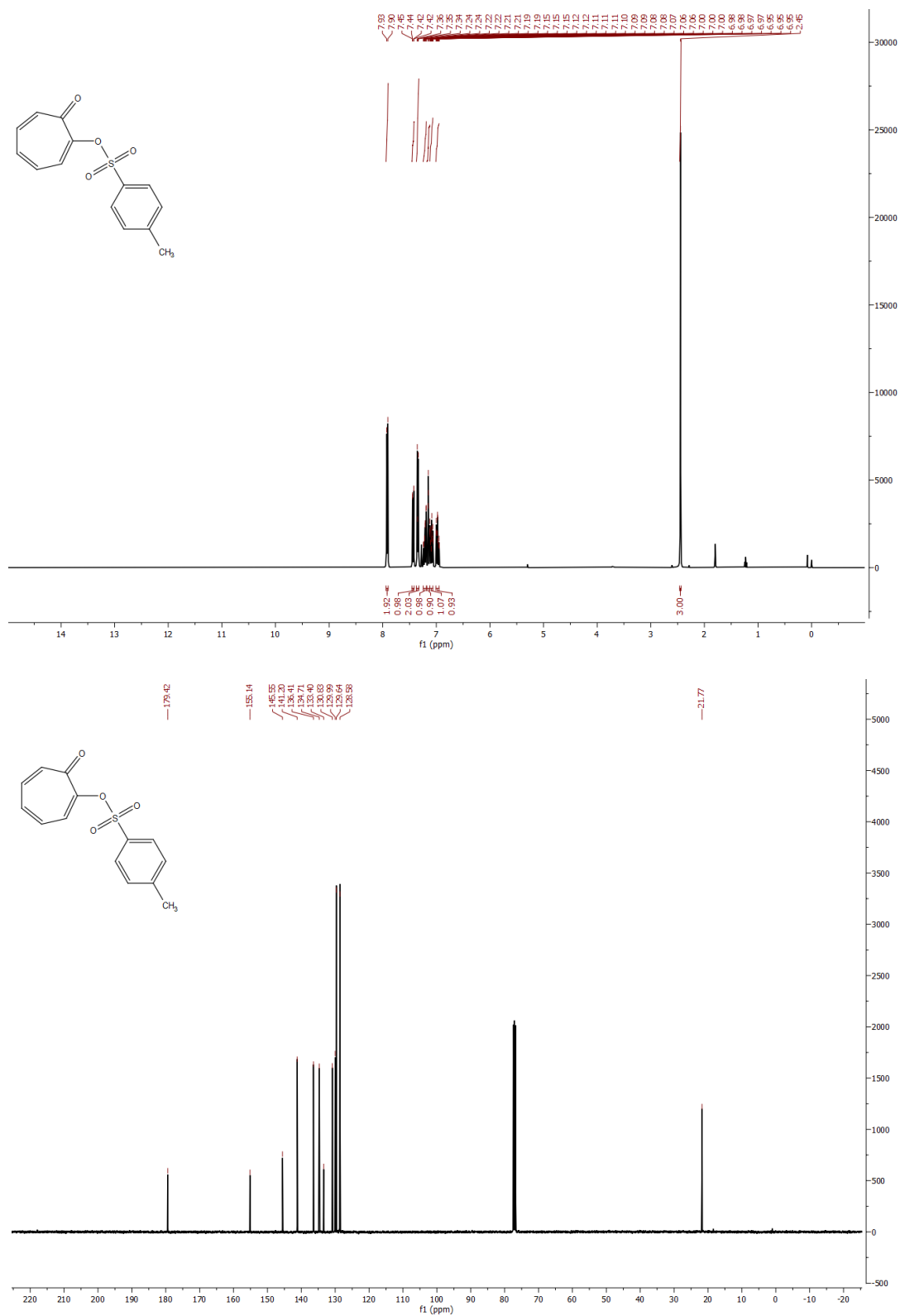


Figure S1. ^1H (top) and ^{13}C (bottom) NMR spectra of 2-tolylsulfonyloxypone (Ts-TP) in CDCl_3 .

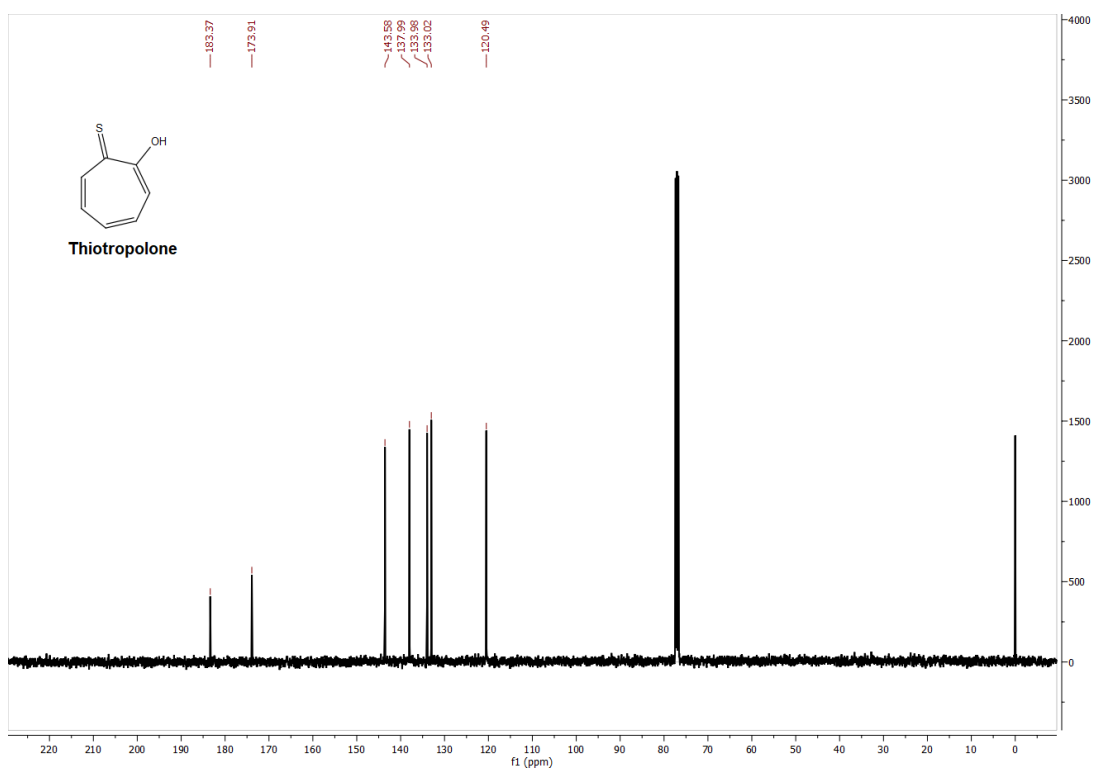
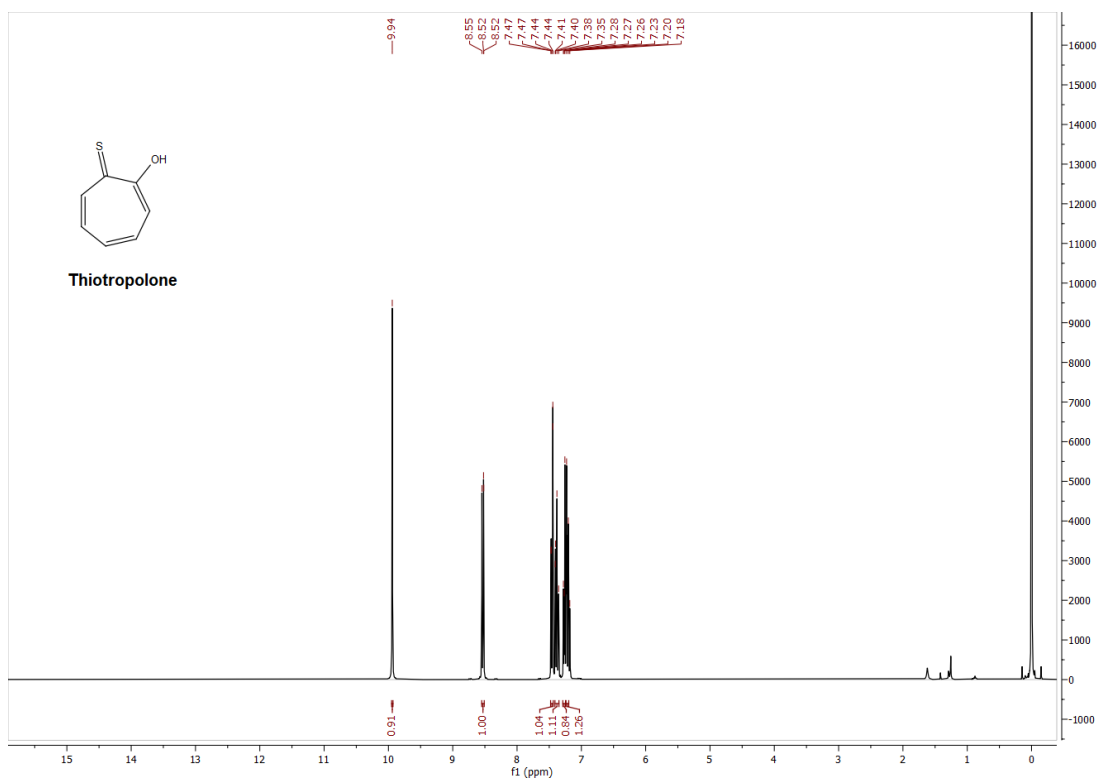


Figure S2. ¹H (top) and ¹³C (bottom) NMR spectra of thiotropolone (TT) in CDCl₃.

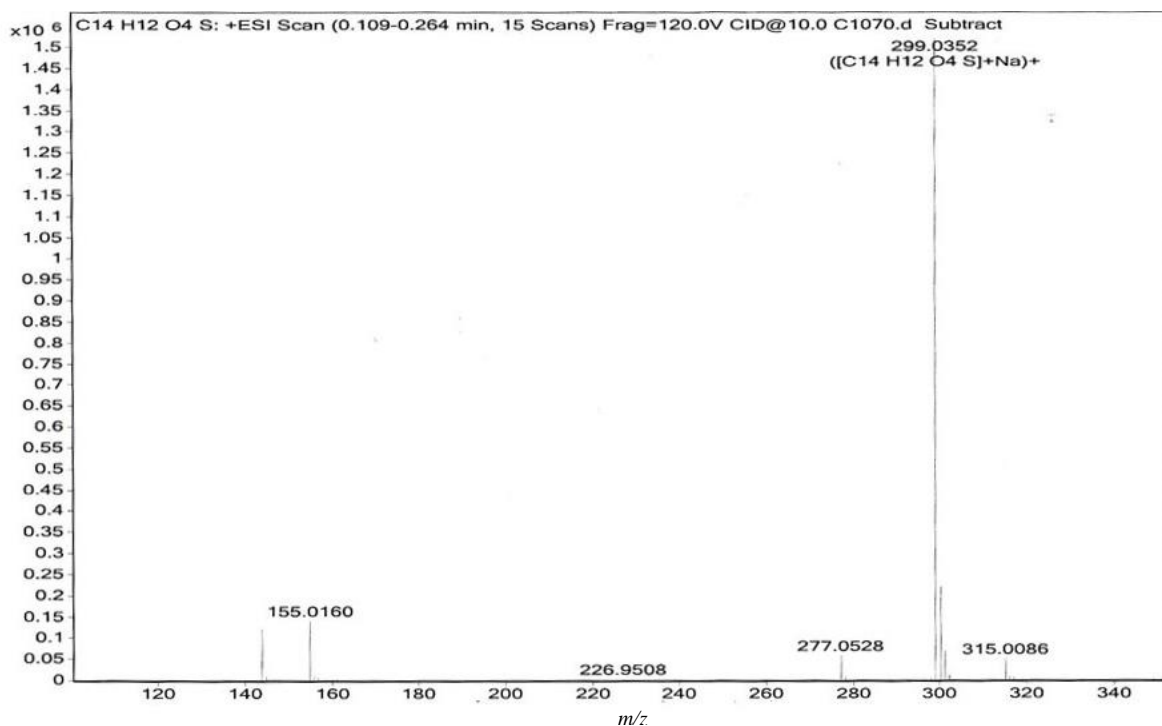


Figure S3. Electrospray ionization mass spectrum in positive-ion mode (HRMS-ESI⁺) of 2-tolylsulfonyloxypone (**Ts-TP**).

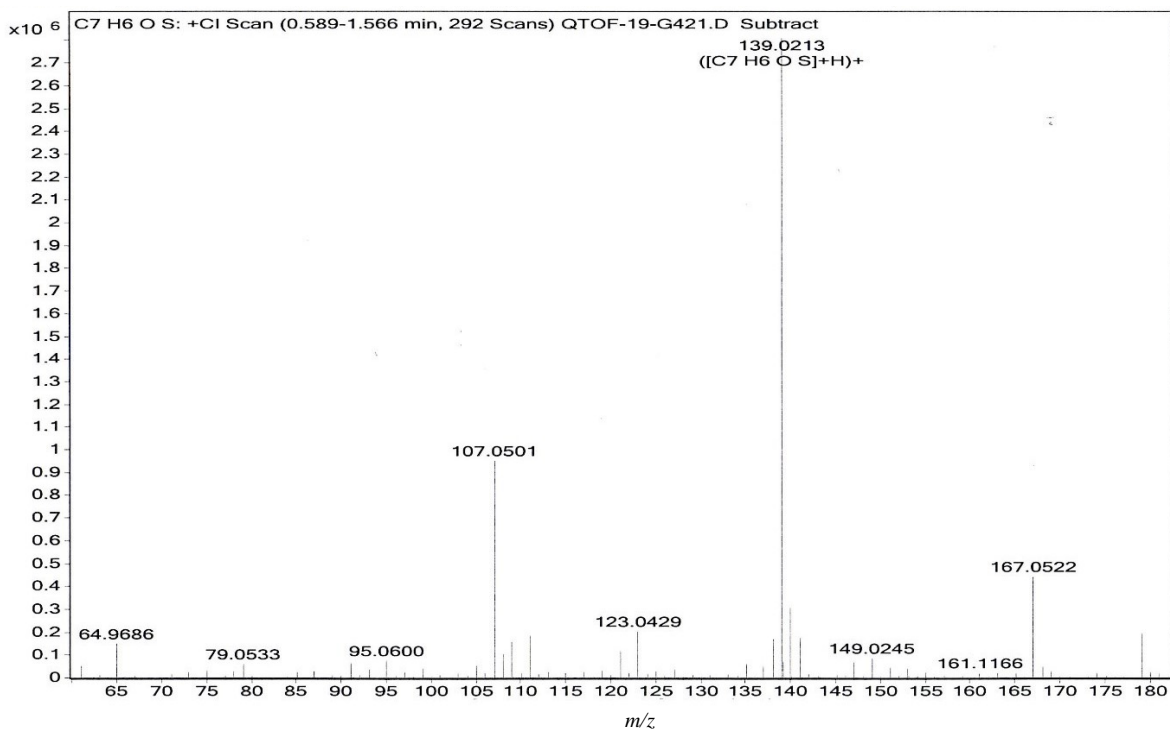


Figure S4. Chemical ionization mass spectrum in positive-ion mode (HRMS-CI⁺) of thiotropone (**TT**).

2.2 IR Spectra and IRC graphs

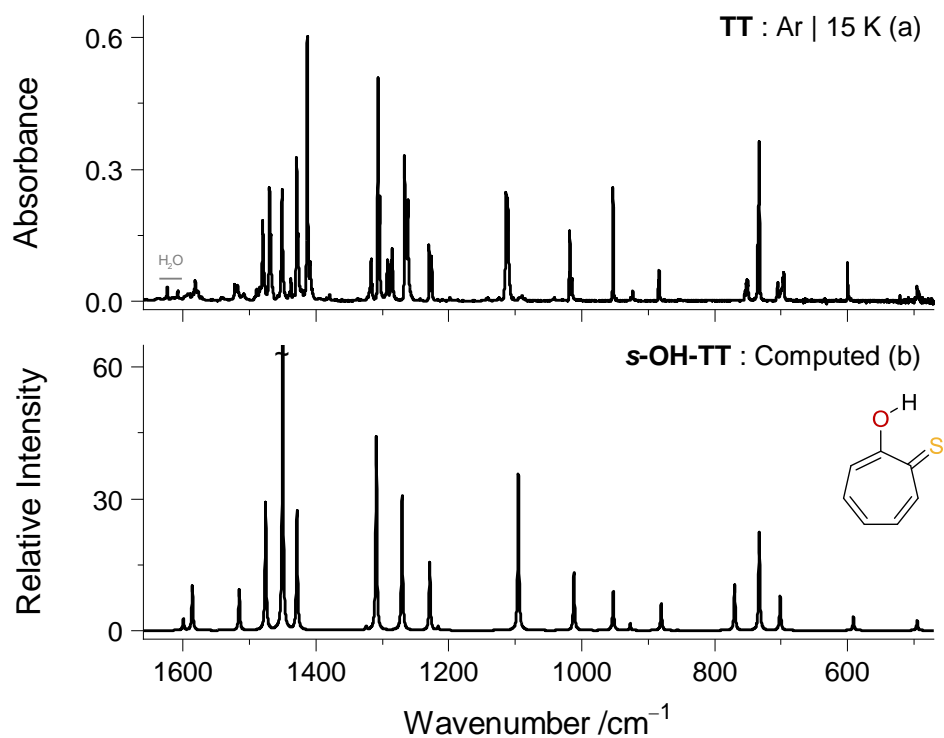


Figure S5. (a) Experimental mid-IR spectrum of thiotropolone (**TT**) in an argon matrix at 15 K. (b) Simulated IR spectrum of *syn*-OH thiotropolone (**s-OH-TT**) based on vibrational data computed at the B3LYP/6-311+G(2d,p) level of theory. Note that some Fermi resonance or overtone bands, appearing in the 1500–1250 cm⁻¹ region, are not described by the computed harmonic IR spectrum (more details are given in Table S1).

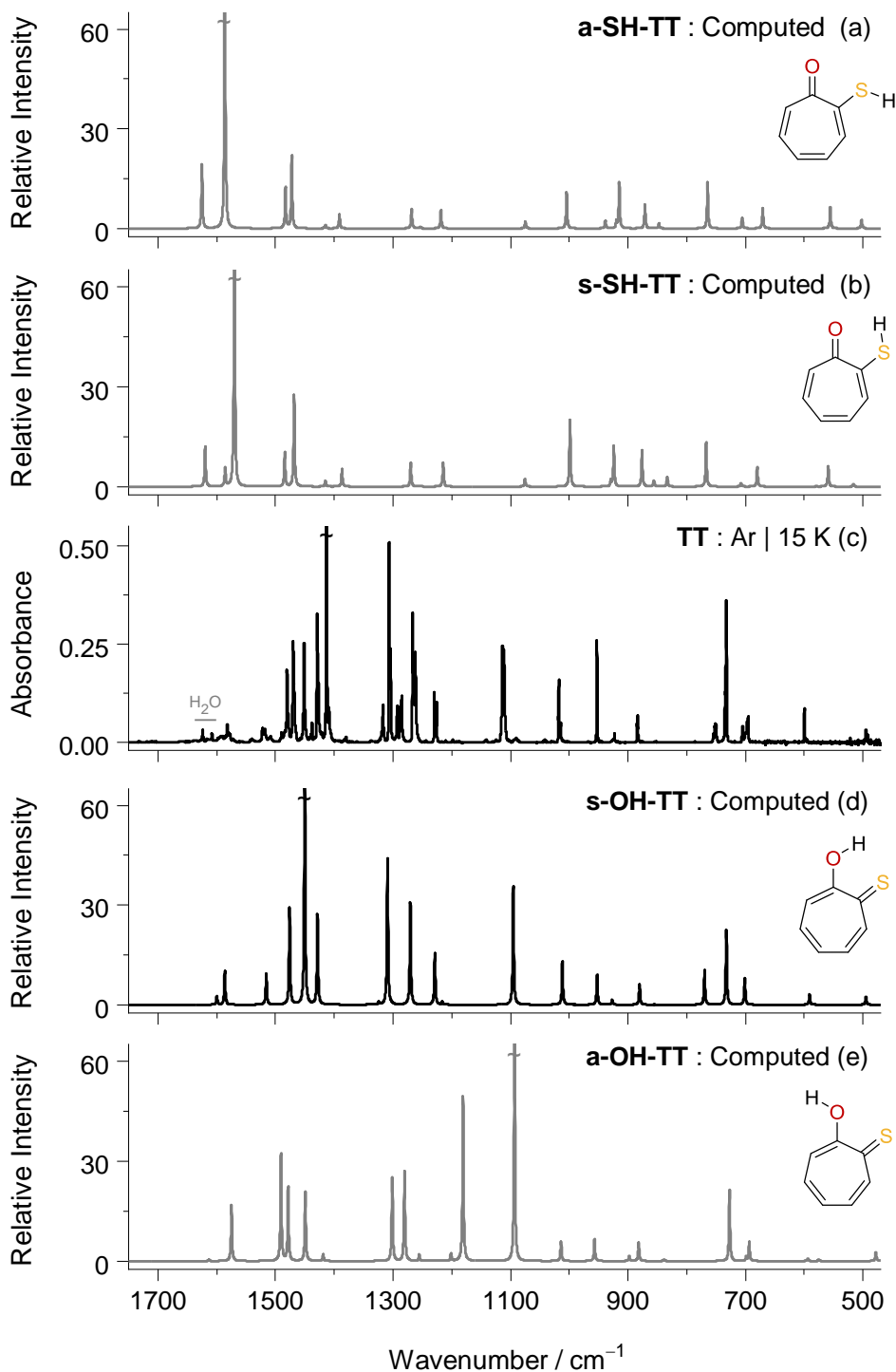


Figure S6. (a,b) Simulated IR spectra of *anti*-SH and *syn*-SH thiol forms of thiotropolone (**a-SH-TT** and **s-SH-TT**) based on vibrational data computed at the B3LYP/6-311+G(2d,p) level of theory. (c) Experimental mid-IR spectrum of thiotropolone (**TT**) in argon matrix at 15 K. (d,e) Simulated IR spectra of *syn*-OH and *anti*-OH forms of thiotropolone (**s-OH-TT** and **a-OH-TT**) computed at the B3LYP/6-311+G(2d,p) level of theory.

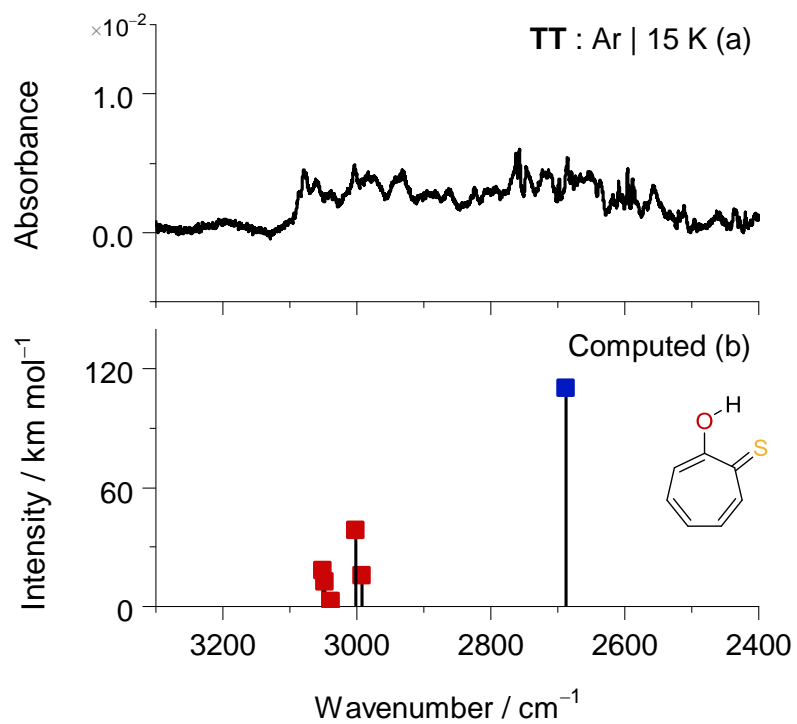


Figure S7. (a) Experimental mid-IR spectrum of thiotropolone (TT) in argon matrix at 15 K. (b) Anharmonic wavenumbers (unscaled) and IR intensities of *syn*-OH thiotropolone (s-OH-TT) computed at the B3LYP/6-311+G(2d,p) level of theory. Blue (■) and red (■) squares depict the $\nu(\text{OH})$ and $\nu(\text{CH})$ fundamental stretching modes, respectively.

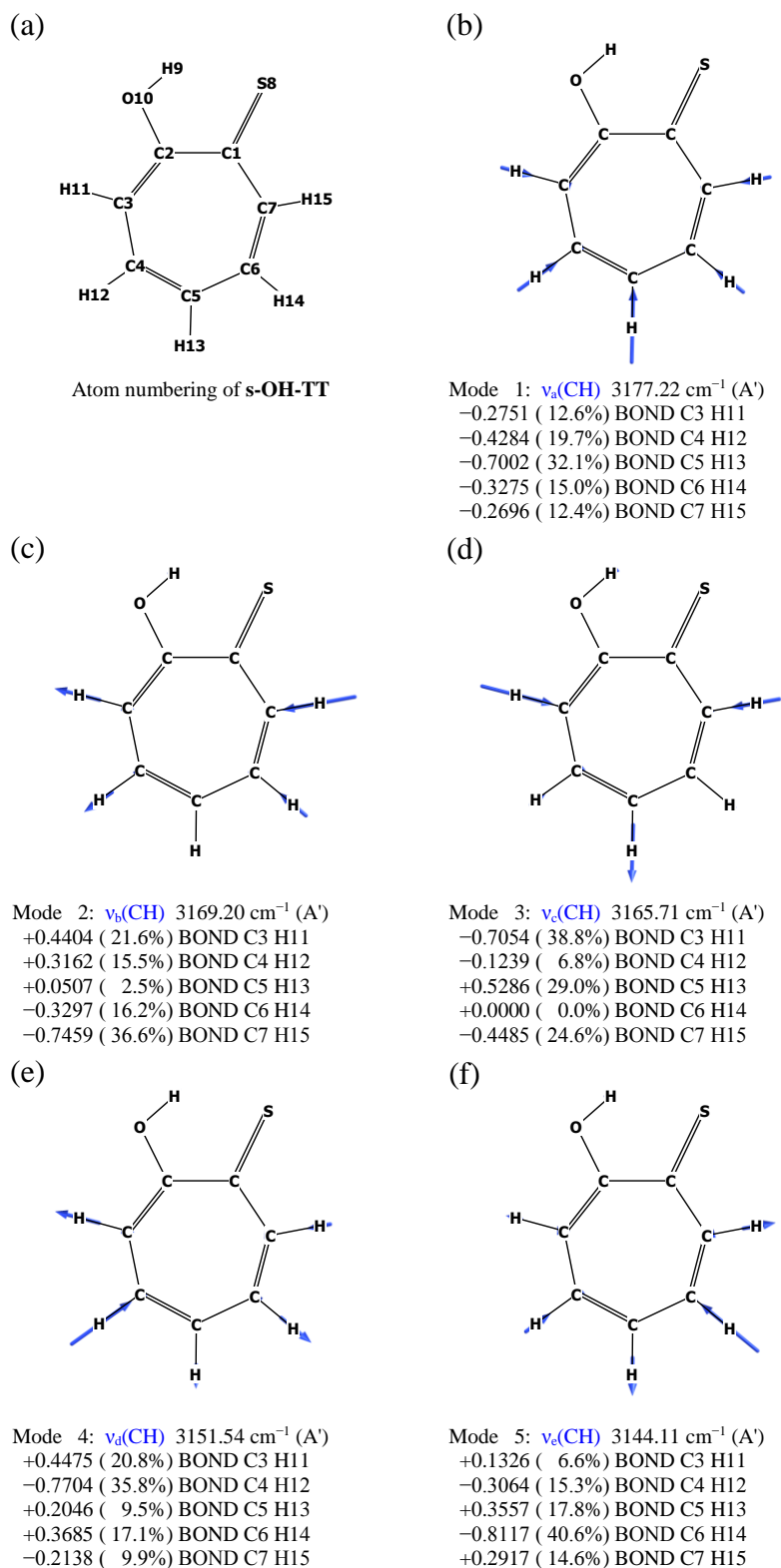


Figure S8. (a) Structure and atom numbering of **s-OH-TT**. (b-f) Molecular vibrations of **s-OH-TT**, computed at the B3LYP/6-311+G(2d,p) level of theory, analyzed using the VMARD (Vibrational Mode Automatic Relevance Determination) approach, as defined in the work of Teixeira and Cordeiro^{S17}. A decomposition of the $\nu(\text{CH})$ modes as a weighted combination of the atomic displacements along the CH bonds is shown. The scaled displacement vectors (blue) for the selected vibrational modes are depicted (using the Chemcraft software^{S21}). The corresponding $2\nu_3(\text{CH})$ overtone was assigned to the 5940 cm^{-1} band, whereas the $2\nu_5(\text{CH})$ overtone with the $[\nu_3(\text{CH}) + \nu_2(\text{CH})]$ and $[\nu_5(\text{CH}) + \nu_4(\text{CH})]$ combination modes were assigned to the 5980 cm^{-1} band observed in the near-IR spectrum of **s-OH-TT** (Figure 1).

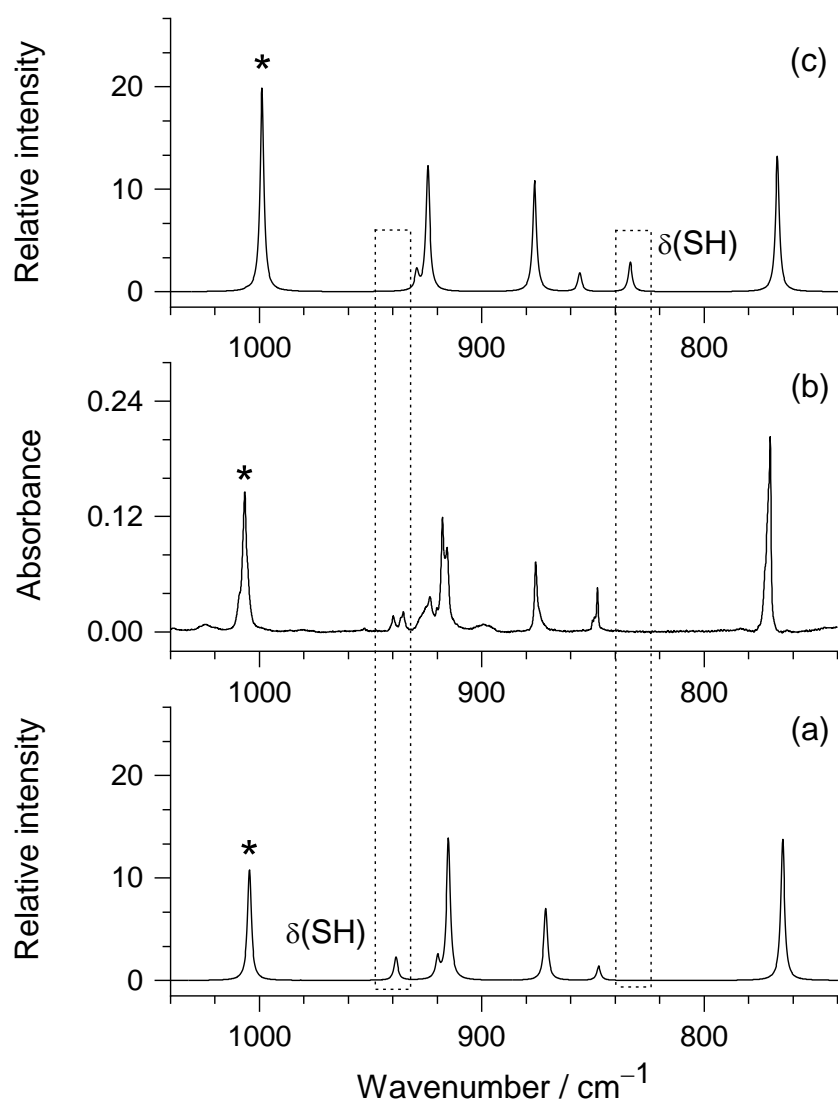


Figure S9. Identification of the thiol tautomeric form (**SH-TT**) produced upon irradiation of **s-OH-TT** at 5980 and 5940 cm^{-1} . (a) Simulated IR spectrum of **a-SH-TT** form based on vibrational data computed at the B3LYP/6-311+G(2d,p) level of theory. (b) Experimental IR spectrum of an argon matrix containing exclusively the same thiol tautomer that was produced by vibrational excitation of **s-OH-TT** (more details are given in experimental and computational methods section). (c) Simulated IR spectrum of **s-SH-TT** form based on vibrational data computed at the B3LYP/6-311+G(2d,p) level of theory. The dotted rectangles are centered at the computed wavenumbers of the vibrational modes with a dominant contribution of the in-plane $\delta(\text{SH})$ bending mode. The asterisks (note relative intensities) appear near the wavenumbers with a minor contribution of the in-plane $\delta(\text{SH})$ bending mode (mixed with the $\nu_r(\text{CC})$ stretching).

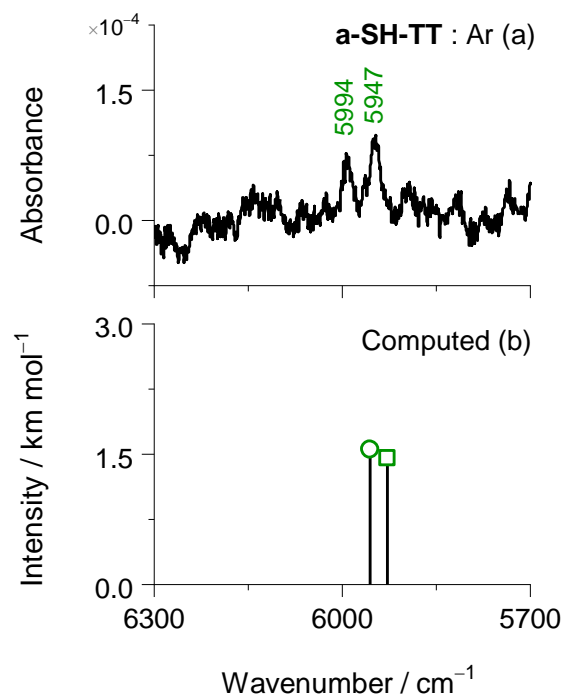


Figure S10. (a) Near-IR spectrum of *anti*-SH thiotropolone (**a-SH-TT**) in argon matrix at 15 K (details about the production of an Ar matrix containing exclusively the **a-SH-TT** tautomer are given in experimental and computational methods section). (b) Anharmonic wavenumbers and IR intensities of **a-SH-TT** computed at the B3LYP/6-311+G(2d,p) level of theory. Open (\square) square depicts the overtone $2\nu_5(\text{CH})$ mode, whereas open (\circ) circle depicts the combination $[\nu_3(\text{CH}) + \nu_4(\text{CH})]$ mode. Only overtone or combination modes with computed infrared intensity $>0.4 \text{ km mol}^{-1}$ are shown.

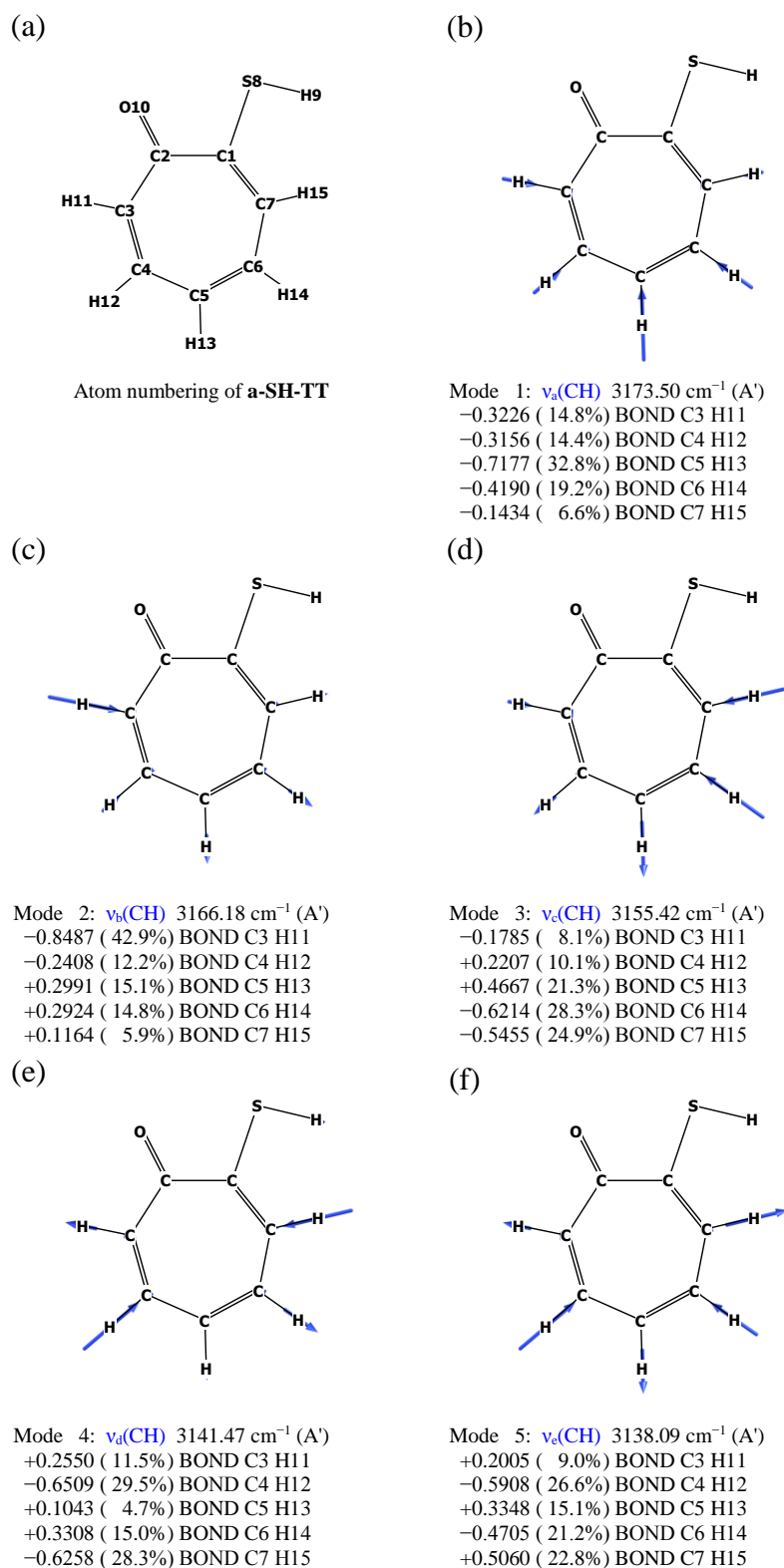


Figure S11. (a) Structure and atom numbering of **a-SH-TT**. (b-f) Molecular vibrations of **a-SH-TT**, computed at the B3LYP/6-311+G(2d,p) level of theory, analyzed using the VMARD (Vibrational Mode Automatic Relevance Determination) approach, as defined in the work of Teixeira and Cordeiro^{S17}. A decomposition of the $\nu(\text{CH})$ modes as a weighted combination of the atomic displacements along the CH bonds is shown. The scaled displacement vectors (blue) for the selected vibrational modes are depicted (using the Chemcraft software^{S21}). The corresponding $2\nu_5(\text{CH})$ overtone and $[\nu_5(\text{CH}) + \nu_4(\text{CH})]$ combination mode were assigned to the 5947 and 5994 cm^{-1} bands observed in the near-IR spectrum of **a-SH-TT** (Figure S10).

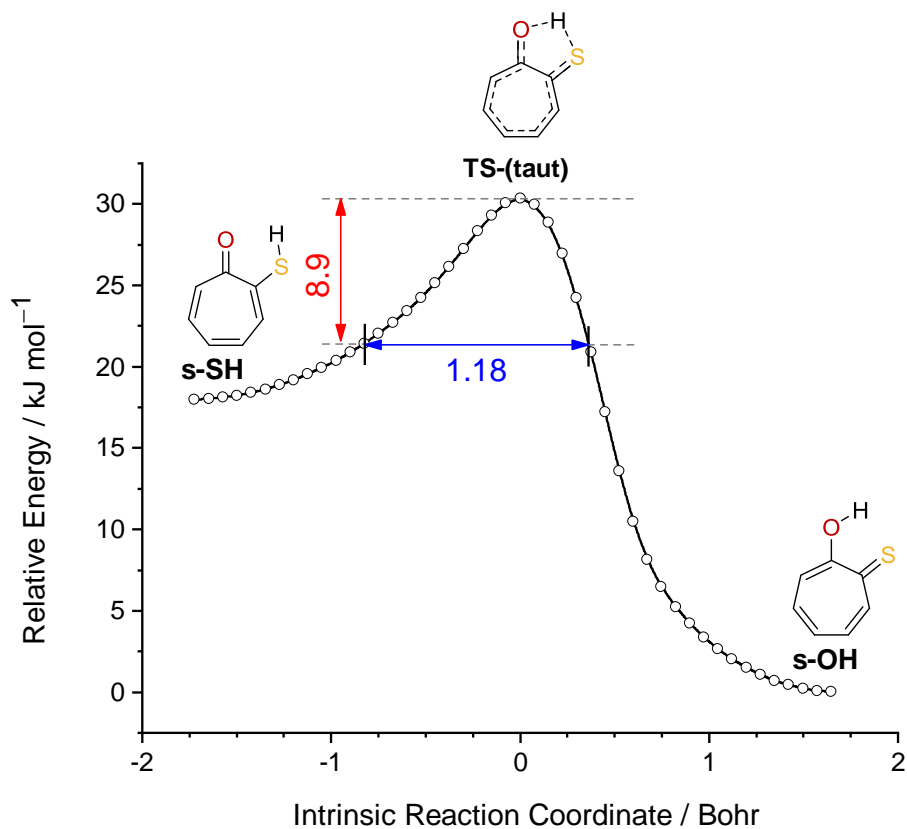


Figure S12. Relative electronic energy as a function of intrinsic reaction coordinate (IRC) for tautomerization of thiol **s-SH-TT** to enol **s-OH-TT** tautomer of thiotropolone computed at the B3LYP/6-311+G(2d,p) level in non-mass-weighted (Cartesian) coordinates. The vertical arrow designates the calculated ZPE-corrected energy of the reactant **s-SH-TT** relative to the transition state **TS-(taut)**. The horizontal arrow designates the barrier width considering the ZPE-corrected energy values of the stationary points superimposed with the pure electronic IRC energy profile.

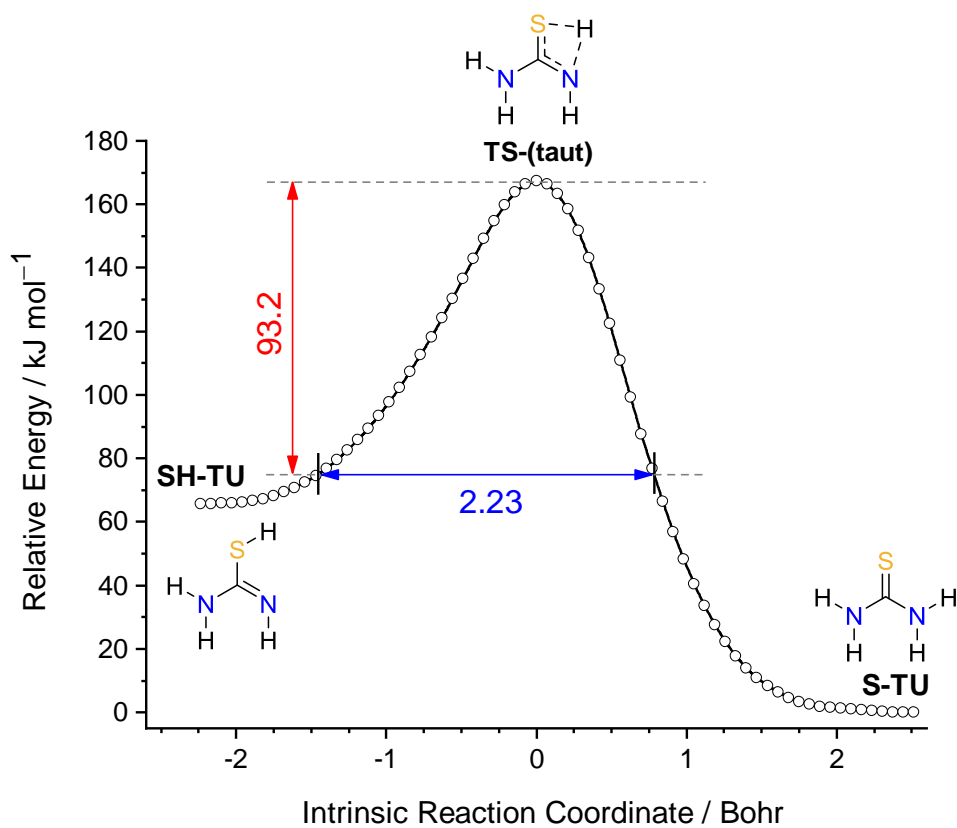


Figure S13. Relative electronic energy as a function of intrinsic reaction coordinate (IRC) for tautomerization of thiol **SH-TU** to thione **S-TU** tautomer of thiourea computed at the B3LYP/6-311+G(2d,p) level in non-mass-weighted (Cartesian) coordinates. The vertical arrow designates the calculated ZPE-corrected energy of the reactant **SH-TU** relative to the transition state **TS-(taut)**. The horizontal arrow designates the barrier width considering the ZPE-corrected energy values of the stationary points superimposed with the pure electronic IRC energy profile.

3. Tables

3.1 Vibrational Data

Table S1. Experimental vibrational wavenumbers and integrated infrared intensities of **s-OH-TT** form of thiotropolone isolated in an argon matrix at 15 K, compared with harmonic wavenumbers ($\tilde{\nu}$ / cm^{-1}) and absolute infrared intensities (A^{th} / km mol^{-1}) computed at the B3LYP/6-311+G(2d,p) level of theory, and vibrational assignment.

Mode N°.	Experimental ^[a]		Calc. ^[b]		Sym.	Approximate Description ^[c]
	Ar, 15 K	<i>I</i>	$\tilde{\nu}$	A^{th}		
A' symmetry						
v ₁	3090–2920	-	3018.4	8.9	A'	v _a (CH)
v ₂		-	3010.7	8.1	A'	v _b (CH)
v ₃		-	3007.4	3.8	A'	v _c (CH)
v ₄		-	2994.0	0.7	A'	v _d (CH)
v ₅		-	2986.9	4.3	A'	v _e (CH)
v ₆	2900–2400	-	2688.1	110.5	A'	v(OH)
v ₇	ov. ^[d]	-	1600.4	7.9	A'	v _a (C=C)
v ₈	1581.9	24.1	1586.4	32.3	A'	v _b (C=C)
v ₉	1522.4 , 1518.2	20.5	1515.9	28.3	A'	$\delta(\text{COH}) - v_b(\text{C}=\text{C})$
v ₁₀	1480.3	56.9	1476.0	92.7	A'	v _c (C=C) + $\delta_a(\text{CH})$
2×v ₃₃	1470.1	78.7			A'	2× $\gamma_e(\text{CH})$
v ₁₁	1451.3	64.5	1450.3	232.1	A'	$\delta_b(\text{CH}) + \delta(\text{COH})$
v ₃₃ +v ₃₄	1437.7	11.7			A'	$\gamma_e(\text{CH}) + \tau_a(\text{ring})$
v ₁₂	1429.1	93.3	1428.8	85.3	A'	$\delta_c(\text{CH})$
2×v ₃₄	1413.3	126.7			A'	2× $\tau_a(\text{ring})$
v ₁₃	1317.1	23.4	1324.3	2.2	A'	v _d (C–C) – v(CO) – $\delta(\text{COH})$
v ₁₄	1306.8 , 1285.4	154.6	1309.3	138.7	A'	v(C–O)
v ₁₅	1266.7 , 1261.8	113.3	1270.3	96.5	A'	$\delta_d(\text{CH})$
v ₁₆	1229.8 , 1225.7	30.2	1229.0	49.2	A'	v(CO) + v _d (C–C)
v ₁₇	-	-	1215.9	2.2	A'	v _e (C–C) + $\delta_e(\text{CH})$
v ₁₈	1113.9 , 1111.3	105.9	1095.8	112.6	A'	v _f (C–C) – v(CS)
v ₁₉	1017.9 , 1014.7	27.5	1012.0	42.0	A'	v _e (C–C) – v(CS)
v ₂₀	952.8	27.0	952.8	28.1	A'	v _g (C–C)
v ₂₁	884.4, 883.5	10.8	880.5	19.2	A'	$\delta_a(\text{ring})$
v ₂₂	697.4, 695.6	23.8	701.5	17.6	A'	v _g (C–C) + $\delta_b(\text{ring})$
v ₂₃	599.8	10.1	591.3	9.7	A'	v(CS) – v _g (C–C)
v ₂₄	495.2 , 492.4	8.9	495.4	7.3	A'	$\delta(\text{CCO})$
v ₂₅	-	-	416.6	1.3	A'	$\delta_c(\text{ring})$
v ₂₆	-	-	334.6	6.6	A'	$\delta_d(\text{ring})$
v ₂₇	-	-	308.4	1.7	A'	$\delta(\text{CCS})$
A'' symmetry						
v ₂₈	-	-	1006.7	0.5	A''	$\gamma_a(\text{CH})$
v ₂₉	-	-	991.0	0.05	A''	$\gamma_b(\text{CH})$
v ₃₀	925.4, 923.1	4.7	926.8	4.8	A''	$\gamma_c(\text{CH})$
v ₃₁	854.1 , 851.9	0.7	855.4	0.2	A''	$\gamma_d(\text{CH})$
v ₃₂	754.2, 751.0	17.9	769.6	32.1	A''	τOH
v ₃₃	734.8, 732.6	71.4	733.5	71.8	A''	$\gamma_e(\text{CH})$
v ₃₄	704.9	6.6	700.8	8.3	A''	$\tau_a(\text{ring})$
v ₃₅	-	-	582.3	0.2	A''	$\tau_b(\text{ring})$
v ₃₆	-	-	390.7	2.3	A''	$\tau_c(\text{ring})$
v ₃₇	-	-	338.9	0.8	A''	$\tau_d(\text{ring})$
v ₃₈	-	-	166.6	0.02	A''	$\gamma(\text{CO}) - \gamma(\text{CS})$
v ₃₉	-	-	92.6	0.1	A''	$\gamma(\text{CS}) + \gamma(\text{CO})$

[a] Experimental intensities (*I*) were normalized in such a way that the sum of integrated experimental intensities (*I*, in arbitrary units) in the 1590-480 cm^{-1} frequency range would be equal to the sum of the corresponding harmonic infrared intensities (A^{th} , in km mol^{-1}) of the two arrays [$\Sigma(v_8:v_{24}) + \Sigma(v_{30}:v_{34})$]

computed at the B3LYP/6-311+G(2d,p) level of theory; [b] Computed harmonic wavenumbers were multiplied by 0.950 (above 2800 cm^{-1}) or 0.979 (below 2000 cm^{-1}) and are expressed in cm^{-1} . The wavenumber and the frequency of the strongly anharmonic $\nu(\text{OH})$ mode were taken from the anharmonic calculations (not scaled). For the split bands, the wavenumbers corresponding to the more intense component are shown in bold; [c] Approximate descriptions are based on visualization of normal vibrations (using the Chemcraft software^{S21}); [d] The band ν_7 marked "ov." is predicted to appear near, and overlapped with the band due to monomeric H_2O in an Ar matrix (see Michaut et al.^{S22}); [e] The suggested assignments of the overtones and combination modes (in the 1500-1400 cm^{-1} frequency range) are based on the experimentally observed wavenumbers of the respective fundamental modes.

Table S2. Experimental vibrational wavenumbers and integrated infrared intensities of **a-SH-TT** form of thiotropolone isolated in an argon matrix at 15 K, compared with harmonic wavenumbers ($\tilde{\nu}$ / cm^{-1}) and absolute infrared intensities (A^{th} / km mol^{-1}) computed at the B3LYP/6-311+G(2d,p) level of theory, and vibrational assignment.

Mode N°.	Experimental ^[a]		Calc. ^[b]		Sym.	Approximate Description ^[c]
	Ar, 15 K	<i>I</i>	$\tilde{\nu}$	A^{th}		
A' symmetry						
ν_1		-	3014.8	11.1	A'	$\nu_a(\text{CH})$
ν_2	3090–2850	-	3007.9	9.0	A'	$\nu_b(\text{CH})$
ν_3		-	2997.6	8.2	A'	$\nu_c(\text{CH})$
ν_4		-	2984.4	0.4	A'	$\nu_d(\text{CH})$
ν_5		-	2981.2	10.1	A'	$\nu_e(\text{CH})$
ν_6		-	2530.6	7.7	A'	$\nu(\text{SH})$
ν_7	1627.7	79.3	1625.1	60.0	A'	$\nu_a(\text{C}=\text{C})$
FR (a)	1602.3 , 1600.5	67.0				FR ^[d] ν_8 with [$\nu_{30}+\nu_{33}$]
FR (b)	1593.6	65.0				FR ^[d] ν_8 with [$\nu_{21}+\nu_{22}$]
ν_8 (c)	1586.7	134.1	1586.2	249.0	A'	$\nu(\text{C}=\text{O})$
ν_9 (d)	1565.3 shoulder	11.0	1584.5	19.7	A'	$\nu_b(\text{C}=\text{C})$
$2\times\nu_{32}$	1540.1	5.1				
ν_{10}	1490.2 , 1482.3	77.0	1482.6	40.1	A'	$\nu_c(\text{C}=\text{C}) - \delta_a(\text{CH})$
ν_{11}	1470.5	37.9	1472.4	67.6	A'	$\delta_a(\text{CH}) - \nu_d(\text{C}-\text{C})$
ν_{12}	1413.1	1.6	1414.9	3.0	A'	$\delta_b(\text{CH})$
ν_{13}	1393.5	14.8	1391.1	12.9	A'	$\delta_c(\text{CH}) + \nu_d(\text{C}-\text{C})$
ν_{14}	1277.0	7.0	1268.2	18.5	A'	$\delta_d(\text{CH}) - \nu_e(\text{C}-\text{C})$
ν_{15}	1255.8	1.0	1254.1	1.3	A'	$\delta_e(\text{CH})$
ν_{16}	1219.2	6.3	1218.6	17.4	A'	$\nu_e(\text{C}-\text{C}) + \delta_c(\text{CH})$
ν_{17}	1078.9	5.7	1074.8	6.3	A'	$\nu_e(\text{C}-\text{C}) + \delta_d(\text{CH})$
ν_{18}	1006.6	37.2	1004.7	33.9	A'	$\nu_f(\text{C}-\text{C}) - \delta(\text{SH})$
ν_{19}	935.3 , 939.8	7.1	939.4	7.5	A'	$\delta(\text{SH}) + \nu_f(\text{C}-\text{C})$
ν_{20}	917.7 , 915.6	34.5	914.9	43.2	A'	$\nu_g(\text{C}-\text{C}) - \delta_a(\text{ring})$
ν_{21}	875.7	12.7	871.2	22.2	A'	$\delta_b(\text{ring})$
ν_{22}	717.6	6.2	705.7	10.0	A'	$\nu_a(\text{C}-\text{C}) + \delta_a(\text{ring})$
ν_{23}	563.5 , 561.8	26.3	555.8	20.2	A'	$\nu(\text{CS})$
ν_{24}	512.6	5.5	502.5	8.4	A'	$\delta(\text{CCO})$
ν_{25}	-	-	407.0	4.5	A'	$\delta_c(\text{ring})$
ν_{26}	-	-	319.9	0.8	A'	$\delta_d(\text{ring})$
ν_{27}	-	-	236.8	5.2	A'	$\delta(\text{CCS})$
A'' symmetry						
ν_{28}	-	-	1007.0	0.2	A''	$\gamma_a(\text{CH})$
ν_{29}	-	-	982.1	0.03	A''	$\gamma_b(\text{CH})$
ν_{30}	923.3 , 925.4 sh	14.7	919.4	6.5	A''	$\gamma_c(\text{CH})$
ν_{31}	848.0 , 849.3	5.6	847.4	4.5	A''	$\gamma_d(\text{CH})$
ν_{32}	770.2	37.8	765.1	43.5	A''	$\tau_a(\text{ring}) - \gamma_e(\text{CH})$
ν_{33}	673.0	19.2	671.1	18.8	A''	$\gamma_e(\text{CH}) + \tau_a(\text{ring})$
ν_{34}	-	-	567.4	0.0003	A''	$\tau_b(\text{ring})$
ν_{35}	-	-	405.3	7.2	A''	τSH
ν_{36}	-	-	347.2	3.2	A''	$\tau_c(\text{ring})$
ν_{37}	-	-	324.9	0.6	A''	$\tau_d(\text{ring})$
ν_{38}	-	-	154.3	0.2	A''	$\gamma(\text{CS}) + \gamma(\text{CO})$
ν_{39}	-	-	66.3	4.5	A''	$\gamma(\text{CO}) - \gamma(\text{CS})$

[a] Experimental intensities (*I*) were normalized in such a way that the sum of integrated experimental intensities (*I*, in arbitrary units) in the 1630–480 cm^{-1} frequency range would be equal to the sum of the corresponding harmonic infrared intensities (A^{th} , in km mol^{-1}) of the two arrays [$\Sigma(\nu_7:\nu_{24}) + \Sigma(\nu_{30}:\nu_{33})$] computed at the B3LYP/6-311+G(2d,p) level of theory; [b] Computed harmonic wavenumbers were multiplied by 0.950 (above 2800 cm^{-1}) or 0.979 (below 2000 cm^{-1}) and are expressed in cm^{-1} . The wavenumber and the frequency of the $\nu(\text{SH})$ mode of the **a-SH-TT** form were taken from the anharmonic calculations (not scaled), by analogy with the $\nu(\text{OH})$ mode of the **s-OH-TT** form. For the split bands, the wavenumbers corresponding to the more intense component are shown in bold; [c] Approximate descriptions are based on visualization of normal vibrations (using the Chemcraft software^{S21}); [d] FR

stands for Fermi-resonance. The suggested FR combinations (tentative) are based on the experimentally observed wavenumbers of the respective fundamental modes. The sum of experimental integrated infrared intensities of the multiplet band in the 1650-1550 cm^{-1} frequency range [marked **(a)-(d)**], where $\nu(\text{C=O})$ and $\nu(\text{C=C})$ bands appear, corresponds to the sum of theoretical intensities due to ν_8 and ν_9 .

3.2 Computed Energies

Table S3. Electronic energies (E_{elec} , Hartree), zero-point energies (E_{ZPE} , Hartree), Gibbs free energies at 298.15 K (G_{298} , Hartree), relative zero-point corrected energies (ΔE_0 , kJ mol^{-1}) and relative Gibbs free energies at 298.15 K (ΔG_{298} , kJ mol^{-1}), calculated at different levels of theory for the most relevant isomers of thiotropolone (**TT**).

		s-OH-TT	a-OH-TT	s-SH-TT	a-SH-TT
CBS-QB3	E_{elec}	-742.81143	-742.79095	-742.80489	-742.80139
	E_{ZPE}	0.11128	0.11118	0.10805	0.10830
	G_{298}	-742.73246	-742.71280	-742.72959	-742.72596
	ΔE_0	0.0	53.5	8.7	18.5
	ΔG_{298}	0.0	51.6	7.5	17.1
MP2/a	E_{elec}	-742.56869	-742.54633	-742.56014	-742.55537
	E_{ZPE}	0.11330	0.11298	0.10956	0.10988
	G_{298}	-742.48768	-742.46639	-742.48335	-742.47841
	ΔE_0	0.0	57.9	12.6	26.0
	ΔG_{298}	0.0	55.9	11.4	24.3
MP2/b	E_{elec}	-742.39449	-742.37247	-742.38685	-742.38198
	E_{ZPE}	0.11206	0.11165	0.10853	0.10860
	G_{298}	-742.31500	-742.29502	-742.31146	-742.30733
	ΔE_0	0.0	56.7	10.8	23.8
	ΔG_{298}	0.0	52.5	9.3	20.1
B2PLYP-GD3BJ/a	E_{elec}	-743.48042	-743.45828	-743.47378	-743.46923
	E_{ZPE}	0.11305	0.11291	0.10967	0.10994
	G_{298}	-743.39963	-743.37836	-743.39682	-743.39213
	ΔE_0	0.0	57.7	8.6	21.2
	ΔG_{298}	0.0	55.8	7.4	19.7
B2PLYP-GD3BJ/b	E_{elec}	-743.41461	-743.39227	-743.40810	-743.40333
	E_{ZPE}	0.11243	0.11222	0.10912	0.10926
	G_{298}	-743.33454	-743.31328	-743.33183	-743.32717
	ΔE_0	0.0	58.1	8.4	21.3
	ΔG_{298}	0.0	55.8	7.1	19.4
B2PLYP/b	E_{elec}	-743.40010	-743.37791	-743.39356	-743.38884
	E_{ZPE}	0.11237	0.11216	0.10906	0.10920
	G_{298}	-743.32008	-743.29896	-743.31735	-743.31273
	ΔE_0	0.0	57.7	8.5	21.2
	ΔG_{298}	0.0	55.5	7.2	19.3

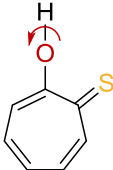
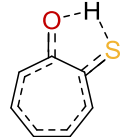
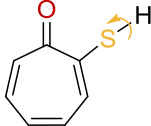
Basis set: a = 6-311++G(3df,3pd) and b = 6-311+G(2d,p). ΔE_0 and ΔG_{298} are given relative to the most stable isomer, **s-OH-TT**.

Table S3 (continued). Electronic energies (E_{elec} , Hartree), zero-point energies (E_{ZPE} , Hartree), Gibbs free energies at 298.15 K (G_{298} , Hartree), relative zero-point corrected energies (ΔE_0 , kJ mol^{-1}) and relative Gibbs free energies at 298.15 K (ΔG_{298} , kJ mol^{-1}), calculated at different levels of theory for the most relevant isomers of thiotropolone (**TT**).

		s-OH-TT	a-OH-TT	s-SH-TT	a-SH-TT
B3LYP-GD3BJ/a	E_{elec}	-743.92795	-743.90545	-743.92126	-743.91663
	E_{ZPE}	0.11281	0.11270	0.10949	0.10974
	G_{298}	-743.84738	-743.82574	-743.84446	-743.83970
	ΔE_0	0.0	58.8	8.8	21.7
	ΔG_{298}	0.0	56.8	7.7	20.2
B3LYP-GD3BJ/b	E_{elec}	-743.90766	-743.88476	-743.90086	-743.89597
	E_{ZPE}	0.11247	0.11230	0.10916	0.10931
	G_{298}	-743.82747	-743.80551	-743.82442	-743.81959
	ΔE_0	0.0	59.7	9.2	22.4
	ΔG_{298}	0.0	57.7	8.0	20.7
B3LYP/a	E_{elec}	-743.89687	-743.87474	-743.89014	-743.88563
	E_{ZPE}	0.11267	0.11256	0.10935	0.10959
	G_{298}	-743.81644	-743.79513	-743.81347	-743.80885
	ΔE_0	0.0	57.8	9.0	21.4
	ΔG_{298}	0.0	55.9	7.8	19.9
B3LYP/b	E_{elec}	-743.87661	-743.85408	-743.86976	-743.86500
	E_{ZPE}	0.11232	0.11216	0.10902	0.10916
	G_{298}	-743.79656	-743.77493	-743.79346	-743.78876
	ΔE_0	0.0	58.7	9.3	22.2
	ΔG_{298}	0.0	56.8	8.1	20.5

Basis set: a = 6-311++G(3df,3pd) and b = 6-311+G(2d,p). ΔE_0 and ΔG_{298} are given relative to the most stable isomer, **s-OH-TT**.

Table S4. Relative zero-point corrected energies (ΔE_0 in kJ mol^{-1}) computed at the CBS-QB3, MP2/6-311++G(3df,3pf), B2PLYP/6-311+G(2d,p) and B3LYP/6-311+G(2d,p) levels of theory for the tautomerization (taut) and rotamerization (rot) transition states (TS) involving the most relevant isomeric structures of thiotropolone (**TT**).^a

Structure			
Name	TS-OH(rot)	TS-(taut)	TS-SH(rot)
CBS-QB3	68.5	22.3 (14.8) ^b	44.7 (27.6)
MP2	75.7	15.6 (4.2)	53.6 (29.3)
B2PLYP	75.6	16.1 (8.9)	51.8 (32.5)
B3LYP	76.1	16.7 (8.9)	53.8 (33.5)

^a ΔE_0 values are relative to the most stable isomer **s-OH-TT**. ^b ΔE_0 values in parentheses are relative to the **s-SH-TT** tautomer. ^cThe use of extended basis sets or dispersion corrections has a minimal effect on the DFT results (see Table S5).

Table S5. Electronic energies (E_{elec} , Hartree), zero-point energies (E_{ZPE} , Hartree), Gibbs free energies at 298.15 K (G_{298} , Hartree), relative zero-point corrected energies (ΔE_0 , kJ mol^{-1}) and relative Gibbs free energies at 298.15 K (ΔG_{298} , kJ mol^{-1}), calculated at different levels of theory for the tautomerization (taut) and rotamerization (rot) transition states (TS) involving the most relevant isomers of thiotropolone (**TT**).

		TS-(taut)	TS-OH(rot)	TS-SH(rot)
CBS-QB3	E_{elec}	-742.79774	-742.78389	-742.79018
	E_{ZPE}	0.10609	0.10983	0.10705
	G_{298}	-742.72371	-742.70695	-742.71652
	ΔE_0	22.3	68.5	44.7
	ΔG_{298}	23.0	67.0	41.8
MP2/a	E_{elec}	-742.55794	-742.53781	-742.54221
	E_{ZPE}	0.10803	0.11155	0.10845
	G_{298}	-742.48197	-742.45923	-742.46707
	ΔE_0	14.4	76.5	56.8
	ΔG_{298}	15.0	74.7	54.1
MP2/b	E_{elec}	-742.38343	-742.36448	-742.36998
	E_{ZPE}	0.10693	0.11087	0.10798
	G_{298}	-742.30873	-742.28653	-742.29517
	ΔE_0	15.6	75.7	53.6
	ΔG_{298}	16.5	74.7	52.1
B2PLYP-GD3BJ/a	E_{elec}	-743.46939	-743.45009	-743.45598
	E_{ZPE}	0.10779	0.11153	0.10864
	G_{298}	-743.39359	-743.37147	-743.38068
	ΔE_0	15.2	75.6	52.6
	ΔG_{298}	15.8	73.9	49.7
B2PLYP-GD3BJ/b	E_{elec}	-743.40334	-743.38444	-743.39070
	E_{ZPE}	0.10723	0.11116	0.10834
	G_{298}	-743.32819	-743.30618	-743.31557
	ΔE_0	15.9	75.9	52.0
	ΔG_{298}	16.7	74.5	49.8
B2PLYP/b	E_{elec}	-743.38875	-743.37002	-743.37628
	E_{ZPE}	0.10717	0.11110	0.10829
	G_{298}	-743.31365	-743.29183	-743.30123
	ΔE_0	16.1	75.6	51.8
	ΔG_{298}	16.9	74.2	49.5

Basis set: a = 6-311++G(3df,3pd) and b = 6-311+G(2d,p). ΔE_0 and ΔG_{298} are given relative to the most stable isomer, **s-OH-TT**.

Table S5 (continued). Electronic energies (E_{elec} , Hartree), zero-point energies (E_{ZPE} , Hartree), Gibbs free energies at 298.15 K (G_{298} , Hartree), relative zero-point corrected energies (ΔE_0 , kJ mol^{-1}) and relative Gibbs free energies at 298.15 K (ΔG_{298} , kJ mol^{-1}), calculated at different levels of theory for the tautomerization (**taut**) and rotamerization (**rot**) transition states (**TS**) involving the most relevant isomers of thiotropolone (**TT**).

		TS-(taut)	TS-OH(rot)	TS-SH(rot)
B3LYP-GD3BJ/a	E_{elec}	-743.91668	-743.89738	-743.90293
	E_{ZPE}	0.10759	0.11130	0.10842
	G_{298}	-743.84107	-743.81897	-743.82784
	ΔE_0	15.9	76.3	54.1
	ΔG_{298}	16.6	74.6	51.3
B3LYP-GD3BJ/b	E_{elec}	-743.89628	-743.87696	-743.88258
	E_{ZPE}	0.10726	0.11102	0.10816
	G_{298}	-743.82103	-743.79884	-743.80768
	ΔE_0	16.2	76.8	54.5
	ΔG_{298}	16.9	75.2	52.0
B3LYP/a	E_{elec}	-743.88543	-743.86657	-743.87210
	E_{ZPE}	0.10746	0.11116	0.10829
	G_{298}	-743.80995	-743.78829	-743.79724
	ΔE_0	16.4	75.6	53.5
	ΔG_{298}	17.1	73.9	50.4
B3LYP/b	E_{elec}	-743.86506	-743.84616	-743.85180
	E_{ZPE}	0.10713	0.11088	0.10802
	G_{298}	-743.78993	-743.76820	-743.77710
	ΔE_0	16.7	76.1	53.8
	ΔG_{298}	17.4	74.5	51.1

Basis set: a = 6-311++G(3df,3pd) and b = 6-311+G(2d,p). ΔE_0 and ΔG_{298} are given relative to the most stable isomer, **s-OH-TT**.

Table S6. Selected two quanta vibrational levels (overtone and combination modes) of the **s-SH-TT** form of thiotropolone [E = vibrational energy, cm^{-1} ; I = infrared intensity, km mol^{-1}] computed at the B3LYP/6-311+G(2d,p) level of theory.^a

Mode (Quanta)	E(anharm)	I (anharm)	Mode (Quanta)	E(anharm)	I (anharm)
1(2)	6065.530	0.01011728	12(1) + 1(1)	4460.658	0.01108402
2(2)	6027.775	0.36575350	12(1) + 2(1)	4460.480	0.04761090
3(2)	6001.679	0.06119179	12(1) + 3(1)	4439.525	0.00665155
4(2)	5963.335	1.69801134	12(1) + 4(1)	4435.208	0.05162672
5(2)	5921.240	1.21403207	12(1) + 5(1)	4420.023	0.00423581
6(2)	4619.014	0.17324835	13(1) + 1(1)	4430.841	0.00048338
2(1) + 1(1)	6049.488	0.24059942	13(1) + 2(1)	4425.628	0.00979874
3(1) + 1(1)	6020.081	0.25847448	13(1) + 3(1)	4411.961	0.00256722
3(1) + 2(1)	6047.679	0.21391196	13(1) + 4(1)	4401.961	0.01704347
4(1) + 1(1)	6030.647	0.06734982	13(1) + 5(1)	4390.688	0.05981936
4(1) + 2(1)	6030.734	0.26294483	14(1) + 1(1)	4321.052	0.02042022
4(1) + 3(1)	6027.963	0.14385895	14(1) + 2(1)	4311.413	0.04148158
5(1) + 1(1)	6035.329	0.04481346	14(1) + 3(1)	4303.170	0.00411380
5(1) + 2(1)	6039.388	0.00953515	14(1) + 4(1)	4291.068	0.03555672
5(1) + 3(1)	5979.111	0.18964864	14(1) + 5(1)	4279.573	0.00446748
5(1) + 4(1)	5999.200	0.38026611	15(1) + 1(1)	4305.010	0.01132307
6(1) + 1(1)	5432.484	0.00038581	15(1) + 2(1)	4301.807	0.01026776
6(1) + 2(1)	5428.047	0.00037220	15(1) + 3(1)	4285.382	0.01751403
6(1) + 3(1)	5413.778	0.00131978	15(1) + 4(1)	4277.984	0.02427013
6(1) + 4(1)	5403.450	0.00014314	15(1) + 5(1)	4264.782	0.00152601
6(1) + 5(1)	5391.722	0.01517920	16(1) + 1(1)	4263.422	0.01074926
7(1) + 1(1)	4656.608	0.03529635	16(1) + 2(1)	4258.888	0.10336008
7(1) + 2(1)	4660.728	0.02714664	16(1) + 3(1)	4244.528	0.00634173
7(1) + 3(1)	4640.377	0.01779008	16(1) + 4(1)	4232.101	0.17595271
7(1) + 4(1)	4628.143	0.14677174	16(1) + 5(1)	4221.020	0.08908601
7(1) + 5(1)	4615.732	0.07592739	17(1) + 1(1)	4123.623	0.02548298
7(1) + 6(1)	4000.694	0.03534586	17(1) + 2(1)	4119.677	0.02518905
8(1) + 1(1)	4627.177	0.01530271	17(1) + 3(1)	4105.531	0.14875928
8(1) + 2(1)	4621.955	0.02526076	17(1) + 4(1)	4095.803	0.00233959
8(1) + 3(1)	4607.598	0.09031153	17(1) + 5(1)	4083.335	0.02971035
8(1) + 4(1)	4601.776	0.04592008	18(1) + 1(1)	4059.221	0.00000113
8(1) + 5(1)	4582.109	0.21678813	18(1) + 2(1)	4051.729	0.00279428
9(1) + 1(1)	4615.836	0.01438969	18(1) + 3(1)	4042.464	0.00100925
9(1) + 2(1)	4611.998	0.12118112	18(1) + 4(1)	4024.183	0.00135847
9(1) + 3(1)	4600.212	0.00149702	18(1) + 5(1)	4020.199	0.00009857
9(1) + 4(1)	4591.147	0.00946018	19(1) + 1(1)	4045.758	0.09207281
9(1) + 5(1)	4574.137	0.00536600	19(1) + 2(1)	4041.056	0.00995218
10(1) + 1(1)	4531.290	0.03118344	19(1) + 3(1)	4027.152	0.10675278
10(1) + 2(1)	4526.755	0.00514248	19(1) + 4(1)	4016.062	0.00320022
10(1) + 3(1)	4521.018	0.01489156	19(1) + 5(1)	4003.713	0.22527219
10(1) + 4(1)	4501.813	0.01337261	20(1) + 1(1)	4038.694	0.00019395
10(1) + 5(1)	4488.602	0.02615865	20(1) + 2(1)	4037.092	0.00037054
11(1) + 1(1)	4518.226	0.00859683	20(1) + 3(1)	4017.251	0.00005885
11(1) + 2(1)	4507.092	0.17865228	20(1) + 4(1)	4013.268	0.00138675
11(1) + 3(1)	4490.188	0.00078387			
11(1) + 4(1)	4486.154	0.09815322			
11(1) + 5(1)	4469.072	0.00483219			

^a Only values with vibrational energy above 4000 cm^{-1} are presented.

4. References

- (S1) Elagawany, M.; Hegazy, L.; Cao, F.; Donlin, M. J.; Rath, N.; Tavis, J.; Elgendy, B. Identification of 4-isopropyl-thiotropolone as a novel anti-microbial: Regioselective synthesis, NMR characterization, and biological evaluation. *RSC Advances* **2018**, *8*, 29967–29975.
- (S2) Daniel, K. B.; Major Jourden, J. L.; Negoescu, K. E.; Cohenet, S. M. Activation of sulfonate ester based matrix metalloproteinase proinhibitors by hydrogen peroxide. *J. Biol. Inorg. Chem.* **2011**, *16*, 313–323.
- (S3) Machiguchi, T.; Hasegawa, T.; Kano, Y. General synthesis, spectroscopic properties, and dipole moments of 2-substituted trophionones. *Bull. Chem. Soc. Jpn.* **1993**, *66*, 3699–3706.
- (S4) Frisch, M. J.; Trucks, G. W.; Schlegel, H. B.; Scuseria, G. E.; Robb, M. A.; Cheeseman, J. R.; Scalmani, G.; Barone, V.; Petersson, G. A.; Nakatsuji, H.; Li, X.; Caricato, M.; Marenich, A. V.; Bloino, J.; Janesko, B. G.; Gomperts, R.; Mennucci, B.; Hratchian, H. P.; Ortiz, J. V.; Izmaylov, A. F.; Sonnenberg, J. L.; Williams-Young, D.; Ding, F.; Lipparini, F.; Egidi, F.; Goings, J.; Peng, B.; Petrone, A.; Henderson, T.; Ranasinghe, D.; Zakrzewski, V. G.; Gao, J.; Rega, N.; Zheng, G.; Liang, W.; Hada, M.; Ehara, M.; Toyota, K.; Fukuda, R.; Hasegawa, J.; Ishida, M.; Nakajima, T.; Honda, Y.; Kitao, O.; Nakai, H.; Vreven, T.; Throssell, K.; Montgomery, J. A., Jr.; Peralta, J. E.; Ogliaro, F.; Bearpark, M. J.; Heyd, J. J.; Brothers, E. N.; Kudin, K. N.; Staroverov, V. N.; Keith, T. A.; Kobayashi, R.; Normand, J.; Raghavachari, K.; Rendell, A. P.; Burant, J. C.; Iyengar, S. S.; Tomasi, J.; Cossi, M.; Millam, J. M.; Klene, M.; Adamo, C.; Cammi, R.; Ochterski, J. W.; Martin, R. L.; Morokuma, K.; Farkas, O.; Foresman, J. B.; Fox, D. J. *Gaussian 16*, Revision B.01; Gaussian, Inc.: Wallingford CT, 2016.
- (S5) Grimme, S. Semiempirical hybrid density functional with perturbative second-order correlation. *J. Chem. Phys.* **2006**, *124*, 034108.
- (S6) Becke, A. D. Density-functional exchange-energy approximation with correct asymptotic behavior. *Phys. Rev. A* **1988**, *38*, 3098–3100.
- (S7) Becke, D. A. Density-functional thermochemistry. III. The role of exact exchange. *J. Chem. Phys.* **1993**, *98*, 5648–5652.
- (S8) Lee, C. T.; Yang, W. T.; Parr, R. G. Development of the Colle-Salvetti correlation-energy formula into a functional of the electron density. *Phys. Rev. B* **1988**, *37*, 785–789.
- (S9) Vosko, S. H.; Wilk, L.; Nusair, M. Accurate spin-dependent electron liquid correlation energies for local spin density calculations: A critical analysis. *Can. J. Phys.* **1980**, *58*, 1200–1211.
- (S10) Head-Gordon, M.; Pople, J. A.; Frisch, M. J. MP2 energy evaluation by direct methods. *Chem. Phys. Lett.* **1988**, *153*, 503–506.
- (S11) Montgomery Jr., J. A.; Frisch, M. J.; Ochterski, J. W.; Petersson, G. A. A complete basis set model chemistry. VII. Use of the minimum population localization method. *J. Chem. Phys.* **2000**, *112*, 6532–6542.

- (S12) Grimme, S.; Ehrlich, S.; Goerigk, L. Effect of the damping function in dispersion corrected density functional theory. *J. Comput. Chem.* **2011**, *32*, 1456–1465.
- (S13) Fukui, K. The path of chemical reactions - The IRC approach. *Acc. Chem. Res.* **1981**, *14*, 363–368.
- (S14) Nunes, C. M.; Eckhardt, A. K.; Reva, I.; Fausto, R.; Schreiner, P. R. Competitive nitrogen versus carbon tunneling. *J. Am. Chem. Soc.* **2019**, *141*, 14340–14348.
- (S15) Barone, V. Anharmonic vibrational properties by a fully automated second-order perturbative approach. *J. Chem. Phys.* **2005**, *122*, 014108.
- (S16) Bloino, J.; Barone, V. A Second-order perturbation theory route to vibrational averages and transition properties of molecules: General formulation and application to infrared and vibrational circular dichroism spectroscopies. *J. Chem. Phys.* **2012**, *136*, 124108.
- (S17) Teixeira, F.; Cordeiro, M. N. D. S. Improving vibrational mode interpretation using bayesian regression. *J. Chem. Theory Comput.* **2019**, *15*, 456–470.
- (S18) Wentzel, G. Eine verallgemeinerung der quantenbedingungen für die zwecke der wellenmechanik. *Z. Phys.* **1926**, *38*, 518–529.
- (S19) Kramers, H. A. Wellenmechanik und halbzahlige quantisierung. *Z. Phys.* **1926**, *39*, 828–840.
- (S20) Brillouin, L. La mécanique ondulatoire de schrödinger; une méthode générale de résolution par approximations successives. *C. R. Acad. Sci.* **1926**, *183*, 24-26.
- (S21) Zhurko, G. A. ChemCraft, Version 1.8. <http://www.chemcraftprog.com>, 2016.
- (S22) Michaut, X.; Vasserot, A. M.; Abouaf-Marguin, L. Temperature and time effects on the rovibrational structure of fundamentals of H₂O trapped in solid argon: Hindered rotation and RTC satellite. *Vib. Spectrosc.* **2004**, *34*, 83–93.